Received: 21 July 2023 | Revised: 11 October 2023 | Accepted: 13 October 2023

DOI: 10.1002/hyp.15018

RESEARCH ARTICLE

WILEY

Relationship between isotope ratios in precipitation and stream water across watersheds of the National Ecological Observation Network

Zachariah Butler[1,2] | Stephen Good[1,2] | Marja Haagsma[2] | Catalina Segura[1,3] | Huancui Hu[4]

[1]Water Resources Graduate Program, Oregon State University (OSU), Corvallis, Oregon, USA

[2]Biological & Ecological Engineering, OSU, Corvallis, Oregon, USA

[3]Forest Engineering, Resources & Management, OSU, Corvallis, Oregon, USA

[4]Atmospheric Sciences and Global Change Division, Pacific Northwest National Laboratory (PNNL), Richland, Washington, USA

Correspondence
Zachariah Butler, Oregon State University, 124 SW 26th St, Corvallis, OR 97331, USA.
Email: butlerz@oregonstate.edu

Funding information
National Science Foundation, Grant/Award Numbers: 1943574, 1836768, 1802885; U.S. Department of Energy Office of Science BER

Abstract

The timescales associated with precipitation moving through watersheds reveal processes that are critical to understanding many hydrologic systems. Measurements of environmental stable water isotope ratios (δ^2H and $\delta^{18}O$) have been used as tracers to study hydrologic timescales by examining how long it takes for incoming precipitation tracers become stream discharge, yet limited measurements both spatially and temporally have bounded macroscale evaluations so far. In this observation driven study across North American biomes within the National Ecological Observation Network (NEON), we examined $\delta^{18}O$ and δ^2H stable water isotope in precipitation (δP) and stream water (δQ) at 26 co-located sites. With an average 54 precipitation samples and 139 stream water samples per site collected over 2014–2022, assessment of local meteoric water lines and local stream water lines showed geographic variation across North America. Taking the ratio of estimated seasonal amplitudes of δP and δQ to calculate young water fractions (F_{yw}), showed a F_{yw} range from 1% to 93% with most sites having F_{yw} below 20%. Calculated mean transit times (MTT) based on a gamma convolution model showed a MTT range from 0.10 to 13.2 years, with half of the sites having MTT estimates lower than 2 years. Significant correlations were found between the F_{yw} and watershed area, longest flow length, and the longest flow length/slope. Significant correlations were found between MTT and site latitude, longitude, slope, clay fraction, temperature, precipitation magnitude, and precipitation frequency. The significant correlations between water timescale metrics and the environmental characteristics we report share some similarities with those reported in prior studies, demonstrating that these quantities are primarily driven by site or area specific factors. The analysis of isotope data presented here provides important constraints on isotope variation in North American biomes and the timescales of water movement through NEON study sites.

KEYWORDS
gamma function, mean transit time, National Ecological Observatory Network, stable isotopes, watersheds, young water fraction

1 | INTRODUCTION

The timescales associated with precipitation moving through watersheds into streams and rivers are indicative of surface and subsurface hydrologic pathways (McDonnell et al., 2010; McGuire & McDonnell, 2006). Understanding hydrologic pathways is critical to properly estimate the timing of water movement but also the retention, mobility, and fate of water solutes that influence water quality, water management, and environmental biodiversity (Brooks et al., 2010; Clow et al., 2018; Godsey et al., 2010; Good et al., 2015; Maxwell et al., 2016; McGuire & McDonnell, 2006; van Meerveld et al., 2019). The time and speed at which water enters and exits a watershed or group of watersheds determines availability for end users, which in turn affects biodiversity and health of a watershed through the interaction of the surface and subsurface (Goodman et al., 2015; Wagener et al., 2010). Accordingly, the dominant problem in understanding watershed health through the lens of hydrologic connectivity, is how to describe watershed functionality through the retaining and releasing of water from storage (Bansah & Ali, 2019). The associated age of water and the linkages to watershed functionality are critical to ecosystem health due to the connectivity of water availability and quality through hydrologic pathways. Despite important implications for future watershed health, the age of water and connectivity to watershed functionality remain uncertain. In North America, the increasing observation network of hydrologic and other environmental variables allow for a unique opportunity to understand watershed functionality through the lens of water age.

Stable water isotope data (δ^2H and $\delta^{18}O$) provide a powerful tool to study hydrologic connectivity and transit times that are reflective of integrated transport processes within a landscape (Brooks et al., 2014; Capell et al., 2012; Fiorella et al., 2021; Jasechko et al., 2016; Kirchner, 2016a, 2016b; Lutz et al., 2018; McGuire et al., 2005; McGuire & McDonnell, 2006; Stockinger et al., 2016). Isotopic tracers are able to carry a signature of partial evaporation of soil waters and connectivity between soil and deeper subsurface processes (i.e., infiltration mechanisms), thereby linking the response of precipitation becoming discharge (Brooks et al., 2010). Local meteoric water lines (LMWL), local stream water lines (LSWL), deuterium excess ($d\text{-}excess = \delta^2H - 8\delta^{18}O$), and line-conditioned excess ($lc\text{-}excess = \delta^2H - a\delta^{18}O - b$, where a and b are the coefficients of the LMWL) aid in understanding isotope sample variability, evaporative influences, and potential environmental effects at a variety of temporal and spatial scales (Brooks et al., 2014; Halder et al., 2015; Kendall & Coplen, 2001; Landwehr & Coplen, 2006). Hydrologic transit times, as characterized by a transit-time distribution (TTD) and associated mean transit time (MTT), link the variability, shifts, and response between incoming precipitation becoming stream discharge to underlying hydrologic connectivity (Capell et al., 2012; Clow et al., 2018; Hrachowitz et al., 2010; Kirchner, 2016a, 2016b; Lutz et al., 2018; McGuire & McDonnell, 2006; Segura, 2021). Similarly, characterization of the fraction of young water (F_{yw}) in stream water, defined as the fraction of runoff with transit times roughly 2–3 months old (depending on the shape of the underlying TTD), provides another mechanism to understand the timescales of water movement through watersheds (Kirchner, 2016a, 2016b). The implementation of MTT and F_{yw} calculations has varied across the literature due to multiple methodologies that rely on specific spatial and temporal input data (Bansah & Ali, 2019; Capell et al., 2012; von Freyberg et al., 2018; Gabrielli & McDonnell, 2020; Jasechko et al., 2016; Kirchner, 2016a, 2016b; McGuire et al., 2005; van Meerveld et al., 2019; Mosquera et al., 2016; Segura, 2021; Stockinger et al., 2016). There have been many methodologies for understanding water age because different convolution models have been shown to work better or worse in certain types of watersheds, environments, and with different spatial and temporal input data (Kirchner, 2016a, 2016b; McGuire et al., 2005; Stockinger et al., 2016).

There have been several global and regional efforts to understand the relationship between transit times and environmental characteristics (Brooks et al., 2014; Halder et al., 2015; Hrachowitz et al., 2010; Jasechko et al., 2016; Kendall & Coplen, 2001; Lutz et al., 2018; von Freyberg et al., 2018). The Global Network of Isotopes in Precipitation (GNIP) and corresponding Global Network of Isotopes in River (GNIR) have monitored the isotopic composition of precipitation and stream waters for over 60 years worldwide (Halder et al., 2015). The combination of GNIP and GNIR allows a worldwide view of water isotope patterns useful for a range of scientific disciplines and reveal seasonal variations of isotopes in stream waters and precipitation. This information can help provide decision making services for water managers and allow for better understanding of hydrologic processes (Halder et al., 2015). Within the United States (US), 351 surface isotope sites with corresponding precipitation isotopes from 1984 to 1987 within the United States Geological Survey (USGS) National Stream Quality Accounting Network were evaluated by Kendall and Coplen (2001). They showed strong agreement in the isotope spatial characteristics with the spatial characteristics of the GNIP data, allowing their dataset to serve as a proxy for the isotopic compositions in US waterways (Kendall & Coplen, 2001). While these data collections are important to understanding spatially and temporally isotope variation across large scales, they do not provide consistent monitoring of watershed scale processes at distributed sites across different ecological biomes.

Starting in 2012, the National Ecological Observatory Network (NEON) established baseline measurements of precipitation, surface, and vapour water isotopes at all their core sites (Goodman et al., 2015). NEON's goal extends beyond water isotopes to broadly utilize long-term research environments throughout North America to study streams, rivers, and lakes interactions with the atmosphere and other ecological characteristics for at least 30 years (NEON, 2023b). In this study, we present stable water isotope data from co-located precipitation (δP) and stream water (δQ) sites across the continental US and Puerto Rico within NEON. These data are analysed with established methods to understand the hydrologic processes and timescales associated with water movement at each site. Here, our goal is to clarify key hydrologic processes at NEON sites by understanding the movement of water through the surface-subsurface continuum using stable water isotopes. The movement of water at NEON sites has linkages to water cycling, which can provide key insights into

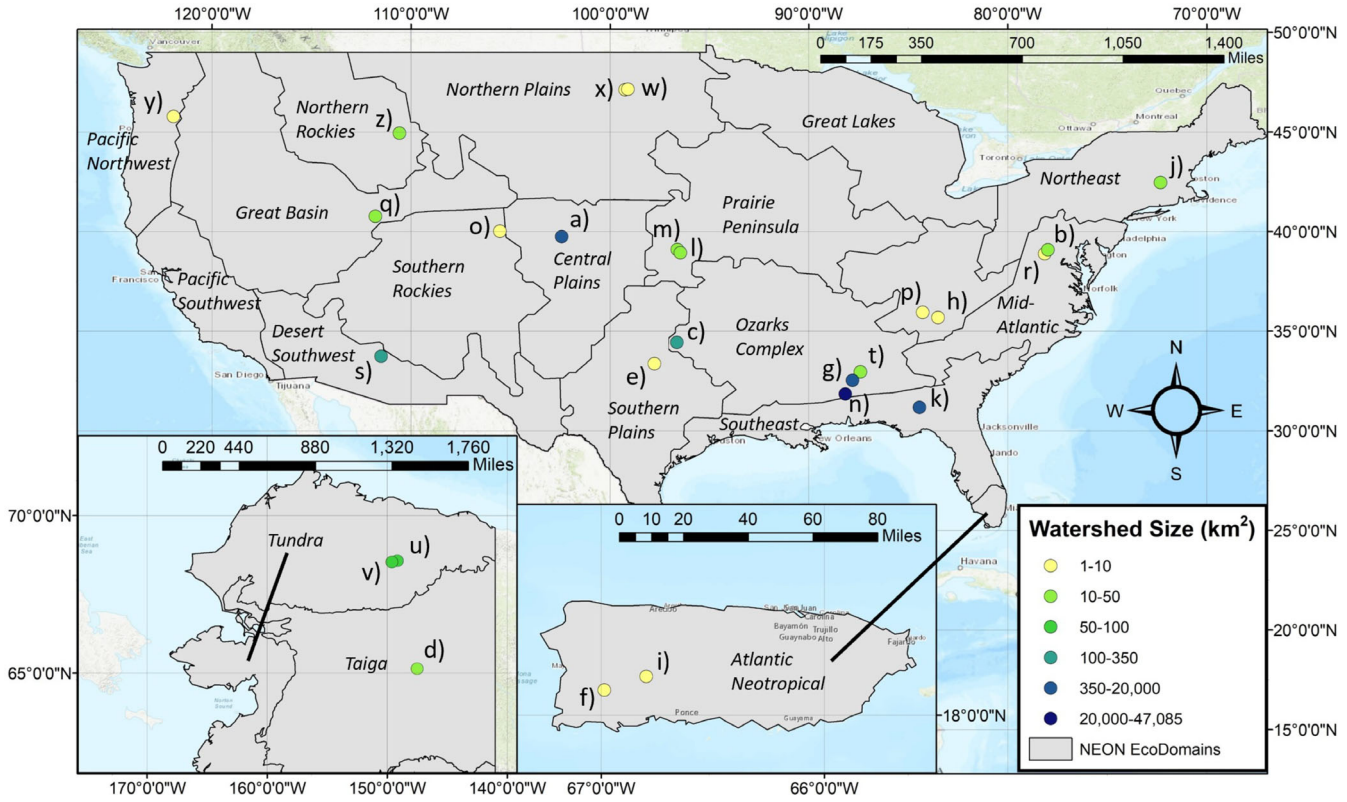

FIGURE 1 Map of 26 National Ecological Observatory Network (NEON) site pairs (lettered a–z) as in Table 1. Each site is colour coded by the watershed size in kilometres squared (km^2) with the NEON ecoclimate domains labelled.

watershed health and aid in future research at NEON sites as well as similar studies. To accomplish our goal, we (1) evaluate the site-specific stable water isotope LMWLs and LSWLs to understand the sample variability, evaporative influences, and any potential environmental effects, (2) evaluate the δP and δQ seasonal cycles and calculate F_{yw}, (3) use δP and δQ information to calculate MTTs based on a gamma convolution model to evaluate the distributions of water transit times at NEON sites, and (4) assess relationships between the LMWL, LSWL, F_{yw}, and MTTs with environmental characteristics, to synthesize findings across the continental US and Puerto Rico.

2 | DATA AND METHODS

2.1 | Study sites and measured data

NEON sites vary in geographic location across the continental US, Hawaii, and Puerto Rico, with vastly different climate and watershed characteristics within the network. Each NEON domain has long-term sites of precipitation (terrestrial) and stream water (aquatic) observations. The aquatic and terrestrial sites are typically co-located (i.e., in close proximity) to support understanding of linkages across terrestrial and aquatic ecosystems and their interactions with the atmosphere (NEON, 2023b). This dataset is unique because both inputs and outputs of hydrologic tracers are actively measured across ecosystems at the continental scale. In this study, NEON terrestrial and aquatic site pairs that are at most 20 kilometres (km) apart are used to allow for observations that are representative of the same environment. Using this 20 km threshold resulted in 26 NEON sites for analysis in this study (Figure 1).

The 26 NEON sites varied in location from Alaska to Puerto Rico and covered nearly all NEON ecoclimatic domains that have a diverse range in geomorphic and climate (environmental) characteristics (Tables 1 and 2). This allows us to capture a wide range of North American ecological and climatic diversity (NEON, 2023b). Watershed areas upstream of the aquatic collection points were obtained from shapefiles via NEON's spatial data and maps portal and analysed within GIS software (ESRI, ArcGIS Version 10.8.2; USGSa TNM Version 2.0, 2023) for geospatial characteristics in concert with a 10 m Digital Elevation Model (DEM) of watershed terrain. Across the NEON sites, watershed area ranges from 1 to 47 085 km^2 with about 75% of the watersheds less than 70 km^2 (NEON, 2023e). See the Sources of Uncertainty and Limitations section about the co-located NEON watersheds that are greater than 100 km^2. The average watershed elevation ranges from 13 to 2908 meters (m) with an average of 588 m. The average slope ranges from 2.2% to 56.3%, with the average slope of 15%. The longest flow path obtained using flow path delineation ranges from 1.3 km to over 530 km with 75% of the watersheds less than 13 km (NEON, 2023e). The soil characteristics were grouped into fractions of clay, silt, and sand, as well as the

TABLE 1 National Ecological Observatory (NEON) site pairs (lettered a–z) environmental characteristics: latitude/longitude (Lat-Lon), state (ST), average elevation (meters (m)), area (area–kilometres (km)), slope (slope–10 m digital elevation model (DEM)), longest flow length (flow length–km), flow length/slope (NEON, 2023a), clay fraction, sand fraction, silt fraction, and porosity.

Site labels (Precip-stream)	Location (Lat, Lon)	ST	Elevation (m)	Area (km)	Slope (10 m DEM)	Flow length (km)	Flow length/slope	Clay fraction	Sand fraction	Silt fraction	Porosity
(a) ARIK-ARIK	39.8, −102.5	CO	1179	2632	2.2	156.0	70.9	0.21	0.44	0.35	0.437
(b) BLAN-LEWI	39.1, −78.0	VA	152	12	7.2	5.3	0.7	0.22	0.52	0.27	0.447
(c) BLUE-BLUE	34.4, −96.6	OK	289	322	3.2	41.0	12.8	0.24	0.50	0.27	0.447
(d) BONA-CARI	65.2, −147.5	AK	230	31	9.6	7.7	0.8	0.20	0.44	0.35	0.437
(e) CLBJ-PRIN	33.4, −97.8	TX	253	4	3.2	12.5	3.9	0.26	0.53	0.21	0.447
(f) CUPE-CUPE	18.1, −67.0	PR	157	4	56.3	4.5	0.1	0.29	0.39	0.32	0.447
(g) DELA-BLWA	32.5, −87.8	AL	22	16 159	12.8	458.9	35.9	0.32	0.32	0.36	0.437
(h) GRSM-LECO	32.5, −87.8	TN	579	9	23.8	5.4	0.2	0.22	0.48	0.29	0.447
(i) GUIL-GUIL	18.2, −66.8	PR	551	10	49.7	6.1	0.1	0.39	0.40	0.21	0.45
(j) HARV-HOPB	42.5, −72.3	MA	203	11.9	7.7	6.1	0.8	0.05	0.78	0.17	0.386
(k) JERC-FLNT	31.2, −84.4	GA	30	14 999	6.15	434.5	70.7	0.16	0.67	0.18	0.419
(l) KONZ-KING	38.9, −96.4	KS	324	13	4.9	5.7	1.2	0.22	0.39	0.40	0.437
(m) KONZ-MCDI	39.1, −96.6	KS	396	23	3	7.7	2.6	0.22	0.39	0.40	0.437
(n) LENO-TOMB	31.8, −88.2	AL	13	47 085	7	530.3	75.8	0.24	0.50	0.26	0.45
(o) NIWO-COMO	40.0, −105.5	CO	2908	4	18.5	7.9	0.4	0.17	0.47	0.37	0.437
(p) ORNL-WALK	36.0, −84.3	TN	264	1	23.1	2.2	0.1	0.22	0.48	0.29	0.447
(q) REDB-REDB	40.8, −111.8	UT	1694	17	25.9	4.2	0.2	0.25	0.49	0.26	0.412
(r) SCBI-POSE	38.9, −78.2	VA	276	2	9.8	1.3	0.1	0.22	0.48	0.30	0.412
(s) SYCA-SYCA	33.8, −111.5	AZ	645	280	33.6	32.3	1.0	0.21	0.54	0.25	0.412
(t) TALL-MAYF	33.0, −87.4	AL	77	14	20.1	4.7	0.2	0.21	0.49	0.29	0.447
(u) TOOL-OKSR	68.7, −149.1	AK	766	58	2.2	10.8	4.9	0.19	0.47	0.35	0.437
(v) TOOL-TOOK	68.6, −149.6	AK	715	68	2.8	8.5	3.0	0.19	0.47	0.35	0.437
(w) WOOD-PRLA	47.1, −99.2	ND	591	4	3.3	2.1	0.6	0.21	0.35	0.44	0.476
(x) WOOD-PRPO	47.1, −99.2	ND	591	2	2.5	2.5	1.0	0.21	0.35	0.44	0.476
(y) WREF-MART	45.8, −121.9	WA	337	6	34.2	2.7	0.1	0.21	0.48	0.31	0.447
(z) YELL-BLDE	45.0, −110.6	WY	2053	38	16.2	12.2	0.8	0.12	0.54	0.34	0.437

Note: See SanClements et al. (2020) supplementary information for the geology at NEON site.

average porosity using the Global Land Data Assimilation System (GLDAS) over a 0.25-degree pixel at each NEON aquatic site (Rodell et al., 2004). The average clay, sand, silt fraction, and porosity respectively across NEON sites is 0.22, 0.47, 0.31, and 0.44. We acknowledge some NEON watersheds are larger than the 0.25-degree pixel and may not be representative of the whole watershed. We obtained NEON watershed geology from SanClements et al. (2020) and took the rock names to translate them into rock types as igneous, metamorphic, or sedimentary. Some rocks had a combination of rock types. We compared various rock types to water timescale metrics and found no correlations using a *t*-test. We exclude geology information from the remainder of the paper and note NEON geology is complex. We recommend future research should investigate rock types correlation to NEON hydrologic processes.

Meteorological variables at the 26 NEON sites were obtained from NEON and the Daily Surface Weather and Climatological Summaries (DAYMET) (NEON, 2023b; Thornton et al., 2022). The average watershed temperature ranges from −9 to 24 Celsius (°C) with an average of 11°C (Table 2). The average watershed precipitation ranges from 262 to 2329 millimeters (mm) with an average of 1014 mm. We noticed highly variable incoming daily precipitation data and acknowledge potential errors via measurement uncertainty through underestimates and overestimates of the NEON precipitation dataset. Thus, we used DAYMET (Version 4 R1) precipitation data because it provides continuous estimates of precipitation in space and time. DAYMET is derived from a collection of algorithms and computer software designed to interpolate and extrapolate from daily meteorological observations to produce gridded estimates of daily weather parameters. DAYMET also covers the continental US and Puerto Rico, which encompasses the NEON sites. We downloaded the 1 km grid pixel over each NEON terrestrial measurement site location spanning the date of the first and last δQ observations (varies per

TABLE 2 National Ecological Observatory (NEON) site pairs (lettered a–z) environmental characteristics: average temperature (°C), and average precipitation magnitude (Precip–millimetres (mm)), intensity (mm/day), and frequency (%).

Precip-stream	Avg temp (°C)	Avg Precip (mm)	Precip intensity (mm/day)	Precip Freq
(a) ARIK-ARIK	10	452	8.5	0.11
(b) BLAN-LEWI	12	976	9.6	0.23
(c) BLUE-BLUE	16	1041	14.6	0.14
(d) BONA-CARI	-3	262	6.0	0.20
(e) CLBJ-PRIN	18	841	14.4	0.12
(f) CUPE-CUPE	24	2050	16.8	0.25
(g) DELA-BLWA	18	1372	15.5	0.20
(h) GRSM-LECO	13	1375	11.0	0.31
(i) GUIL-GUIL	21	1900	14.0	0.38
(j) HARV-HOPB	8	1368	9.9	0.26
(k) JERC-FLNT	19	1311	12.4	0.19
(l) KONZ-KING	12	860	11.8	0.19
(m) KONZ-MCDI	13	921	11.8	0.19
(n) LENO-TOMB	18.1	1386	16.3	0.20
(o) NIWO-COMO	2	841	8.2	0.26
(p) ORNL-WALK	14	1340	12.9	0.28
(q) REDB-REDB	8	751	8.7	0.16
(r) SCBI-POSE	12	1090	10.9	0.30
(s) SYCA-SYCA	21	409	11.2	0.06
(t) TALL-MAYF	17	1379	15.0	0.25
(u) TOOL-OKSR	−9	316	4.8	0.13
(v) TOOL-TOOK	−9	316	4.8	0.13
(w) WOOD-PRLA	4.9	494	8.3	0.14
(x) WOOD-PRPO	4.9	494	8.3	0.14
(y) WREF-MART	10	2329	13.4	0.24
(z) YELL-BLDE	4	481	4.8	0.18

Note: DAYMET was used to calculate precipitation intensity and precipitation frequency.

NEON site) for each individual site from 2014 to 2022. We used DAYMET data to calculate the average precipitation intensity (mean precipitation on days with rain) and average percent of days with precipitation per year. The average precipitation intensity ranges from 4.8 to 16.8 mm/day with an average of 11 mm/day. The average days with precipitation per year range from 6% to 38% with an average of 20%.

NEON isotope data is openly available via their data portal (NEON, 2023a). We downloaded both $\delta^{18}O$ and $\delta^{2}H$ stream (δQ – DP1.20206.001) and precipitation (δP – DP1.00038.001) data. The δP composite samples and δQ grab-samples were collected approximately biweekly and sent to an external laboratory for analysis and archiving (NEON, 2023c, 2023d). The δQ samples are collected, sealed with parafilm to prevent evaporation, and stored on ice within 4 h of sample collection (NEON, 2023d). Isotope ratios in both δQ and δP samples are measured using cavity ringdown spectrometry (NEON, 2023c, 2023d). NEON reports isotope observation uncertainties, where for precipitation (δP) sites and samples, the average uncertainty values for $\delta^{18}O$ are 0.05‰ and $\delta^{2}H$ are 0.35‰. For stream water (δQ) sites and samples, the average uncertainty values for $\delta^{18}O$ are 0.05‰ and $\delta^{2}H$ are 0.33‰ (NEON, 2023c, 2023d). Stream water samples were filtered for outliers following Wassenaar et al., 2018. We eliminated values of δQ that were outside 3 times the interquartile range in order to use acceptable isotope values that would not be skewed by inaccurate or imprecise laboratory performance. On average this eliminated ~3% of δQ data. Table 3 reports the weighted mean values of δP and unweighted δQ data (after filtering for outliers). We use unweighted δQ because NEON does not have reliable discharge data (Rhea et al., 2023). We use weighted $\overline{\delta P}$ to account for differences in isotope values per precipitation amounts so that the outflow composition reflects the mass flux entering the watershed.

There are three NEON sites that are nested in our study area (in Alabama), which are DELA-BLWA (g), LENO-TOMB (n), and TALL-MAYF (t) (Figure 1). Site LENO-TOMB (n) is the largest watershed with sites (g) and (t) nested inside. To account for the large variability of precipitation in site (n), we took the average precipitation and $\overline{\delta P}$ for all three sites to used it for the terrestrial site location LENO (n).

TABLE 3 National Ecological Observatory (NEON) site pairs (lettered a–z) isotope characteristics of the weighted median and standard deviation (Std) $\overline{\delta P}$ ($\overline{O^{18}}$ and $\overline{H^2}$), median (Std) of δQ (O^{18} and H^2), weighted $\overline{\delta P}$ slope (Figure 2), weighted $\overline{\delta P}$ intercept (Figure 2), δQ slope (Figure 2), δQ intercept (Figure 2), and amplitude of δP (A_P) and δQ (A_Q) (Figure 3).

Precip-stream	$\overline{\delta^{18}O\,P}$	$\overline{\delta^{2}H\,P}$	$\delta^{18}O$ Q	$\delta^{2}H$ Q	$\overline{\delta P}$ slope	$\overline{\delta P}$ intercept	δQ slope	δQ intercept	A_P	A_Q
	Median (Std)	Median (Std)	Median (Std)	Median (Std)						
(a) ARIK-ARIK	−8.8 (3.0)	−62.3 (7.9)	−10 (0.6)	−75.5 (3.5)	7.9	7.6	5.4	−21.6	6.38	0.54
(b) BLAN-LEWI	−6.3 (2.5)	−38.2 (6.2)	−7.7 (0.3)	−48.9 (1.2)	7.4	8.2	3.8	−19.9	2.39	0.06
(c) BLUE-BLUE	−5.4 (2.3)	−30.5 (5.5)	−4.9 (0.2)	−28.3 (1.2)	7.1	8.2	4.3	−7.2	2.69	0.07
(d) BONA-CARI	−16.3 (4.0)	−136.5 (11.7)	−19.1 (0.4)	−148 (2.3)	8.8	6.7	5.6	−40.8	2.68	0.17
(e) CLBJ-PRIN	−5 (2.2)	−27.1 (5.2)	−4.2 (0.5)	−25.9 (3.4)	7.1	8.4	5.1	−4.0	2.46	0.35
(f) CUPE-CUPE	−2.9 (1.7)	−11.8 (3.4)	−2.7 (0.3)	−8.3 (1.8)	7.6	10.0	5.1	4.9	1.19	0.14
(g) DELA-BLWA	−3.6 (1.9)	−17.8 (4.2)	−3.9 (0.7)	−21.4 (4.0)	6.0	3.8	5.5	−0.1	0.69	0.37
(h) GRSM-LECO	−5.7 (2.4)	−36 (6.0)	−7 (0.4)	−42.6 (2.7)	8.3	11.3	6.1	0.1	1.84	0.21
(i) GUIL-GUIL	−3.2 (1.8)	−14 (3.7)	−3.1 (0.3)	−11.3 (2.2)	8.4	12.7	5.9	6.6	1.19	0.15
(j) HARV-HOPB	−8.3 (2.9)	−53.4 (7.3)	−8.6 (0.7)	−54.3 (4.8)	8.0	13.2	6.8	3.9	1.91	0.63
(k) JERC-FLNT	−4.1 (2.0)	−20.9 (4.6)	−3.6 (0.5)	−19.3 (3.3)	7.6	10.1	6.5	3.9	0.34	0.32
(l) KONZ-MCDI	−6 (2.4)	−37.6 (6.1)	−6 (0.3)	−38.4 (1.5)	7.8	8.8	4.6	−10.9	3.02	0.03
(m) KONZ-KING	−6 (2.4)	−37.6 (6.1)	−5.5 (0.6)	−35.5 (3.3)	7.8	8.8	5.4	−6.1	3.02	0.16
(n) LENO-TOMB	−4 (2.0)	−19.6 (4.4)	−3.7 (0.7)	−20.6 (4.3)	6.8	7.5	5.5	−0.3	0.57	0.37
(o) NIWO-COMO	−14.9 (3.9)	−115.1 (10.7)	−17.3 (0.6)	−128.9 (4.3)	8.8	16.0	6.6	−13.7	6.08	0.54
(p) ORNL-WALK	−5.8 (2.4)	−34.1 (5.8)	−6.1 (0.3)	−35.5 (1.4)	7.7	10.9	4.3	−9.1	1.92	0.05
(q) REDB-REDB	−14.3 (3.8)	−105.6 (10.3)	−16.5 (0.3)	−122.9 (1.4)	7.0	−6.0	5.0	−41.0	5.44	0.03
(r) SCBI-POSE	−6.5 (2.5)	−39.3 (6.3)	−7.8 (0.3)	−47.2 (2.1)	7.6	10.1	5.8	−2.6	2.45	0.18
(s) SYCA-SYCA	−7.5 (2.7)	−54.1 (7.4)	−8.5 (1.2)	−60.6 (7.5)	6.9	−2.2	6.3	−7.8	4.25	0.83
(t) TALL-MAYF	−4.4 (2.1)	−22.3 (4.7)	−4.3 (0.4)	−21.7 (2.4)	7.1	8.6	5.0	−0.7	0.71	0.13
(u) TOOL-OKSR	−17.8 (4.2)	−147.5 (12.1)	−19.5 (1.0)	−149.4 (7.1)	8.1	−3.8	6.8	−19.7	4.30	2.02
(v) TOOL-TOOK	−17.8 (4.2)	−147.5 (12.1)	−19 (1.0)	−150.7 (7.7)	8.1	−3.8	7.4	−8.5	4.30	0.61
(w) WOOD-PRLA	−10.6 (3.3)	−77.9 (8.8)	−3.7 (1.5)	−45.2 (9.3)	8.2	8.9	6.0	−23.0	2.57	1.01
(x) WOOD-PRPO	−10.6 (3.3)	−77.9 (8.8)	−3.8 (1.8)	−47.1 (10.6)	8.2	8.9	5.9	−24.6	2.57	1.00
(y) WREF-MART	−9.5 (3.1)	−67.5 (8.2)	−10.1 (0.6)	−68.5 (4.2)	7.8	6.2	6.3	−5.4	1.25	0.08
(z) YELL-BLDE	−14.4 (3.8)	−115.9 (10.8)	−19 (0.3)	−144.1 (2.1)	7.4	−10.2	6.1	−28.1	5.99	0.27

This allowed us to consider further upstream impacts on the watershed. Further impacts and limitations on averaging the three sites will be discussed in Section 4.4, Sources of Uncertainty and Limitations.

2.2 | Downscaling of δP and comparing with δQ

NEON δP samples represent aggregated precipitation over an approximately two-week's time scale and to properly understand the changes over a continuous time frame, we statistically downscale the aggregated δP to produce daily δP estimates. The downscaling method combines a deterministic estimate of seasonal variability in δP with stochastically generated daily estimates in δP that are consistent with the covariation of precipitation amount and its isotope ratio (Finkenbiner et al., 2021). The combined deterministic and stochastics time series are then corrected to match the observed low frequency mass inputs. The downscaling was applied to δP for both $\delta^{18}O$ and $\delta^{2}H$ and is openly published via the NEON Daily Isotopic Composition Environmental Exchanges (NEON-DICEE) Dataset (Finkenbiner et al., 2022). Since the downscaling method is stochastic, the analyses conducted here are run across an ensemble of 100 downscaled δP time series per NEON site. This propagates uncertainty in downscaled precipitation estimates through later analyses. We use each ensemble δP in our methods below.

To understand the evaporative and elevation influences within the δP and δQ meteoric water lines, we assessed the local meteoric water lines (LMWL), the local stream water lines (LSWL), and line-conditioned excess (*lc-excess*) (Landwehr & Coplen, 2006). Using a weighted linear regression, the LMWL slope and intercept were fit to precipitation $\overline{\delta^{18}O}$ vs. $\overline{\delta^{2}H}$ samples and DAYMET precipitation amount. The LSWL slope and intercept were fit to stream water $\delta^{18}O$ vs. $\delta^{2}H$ samples. The *lc-excess* allows a greater understanding of the

evaporative influences where the moisture source is measured (δP), relative to where stream water is sampled (δQ). The *lc-excess* is defined as:

$$lc-excess = \delta^2H - a * \delta^{18}O - b \quad (1)$$

where a is the slope and b is the y-intercept of the LMWL.

2.3 | F_{yw} and MTT calculation

Existing F_{yw} and MTT mathematical approaches were used based on Kirchner (2016a, 2016b) and McGuire et al. (2005). The F_{yw} in stream water was calculated using the seasonal cycles of the δP and δQ, by estimating the amplitudes A and phases φ through nonlinear fitting to a sine curve, thereby a simpler metric and less computational involved than TTD (Kirchner, 2016a; Lutz et al., 2018). The sine curves for the precipitation isotope ratio, δP(t) and stream water isotope ratio, δQ(t) are given as:

$$\delta P(t) = A_P \sin(2\pi ft - \varphi_P) + k_P \quad (2a)$$

$$\delta Q(t) = A_Q \sin(2\pi ft - \varphi_Q) + k_Q \quad (2b)$$

where t is time, f is the frequency of the cycle ($f = 1$ year^{-1} for a seasonal cycle), the subscripts P and Q refer to precipitation and stream water, and k is the curve offset. We applied this only for $\delta^{18}O$ isotope data for reporting simplicity. We did the analysis for δ^2H and found very similar results. The F_{yw} from the above equation is defined as amplitude in δQ (A_Q) divided by the amplitude in δP (A_P) (i.e., $F_{yw} = A_Q/A_P$). We used 100 ensemble-member inputs of δP that allowed for the F_{yw} to be estimated 100 times per input.

We employed a convolution approach following McGuire et al. (2005) to estimate a time invariant TTD based on the incoming data of δP, DAYMET precipitation amount, and output data δQ. In the convolution model to estimate stream water isotopes, we used the input precipitation signal (δP) and the output stream water signal (δQ) considering the lag of past inputs δP ($t-\tau$) according to their TTD, $g(\tau)$ (McGuire et al., 2005). The input precipitation signal (δP) was volume weighted by weighing $w(t-\tau)$ using DAYMET precipitation data. This ensured that the stream water composition reflects the mass flux leaving the watershed (McGuire et al., 2005).

$$\delta Q(t) = \frac{\int_0^\infty g(\tau)w(t-\tau)\delta P(t-\tau)d\tau}{\int_0^\infty g(\tau)w(t-\tau)\delta d\tau} \quad (3)$$

We utilized three convolution approaches, which were the gamma probability density function (PDF) distribution, exponential distribution, and power law distribution (Kirchner et al., 2001; Maloszewski & Zuber, 1982; Schumer et al., 2003). In the gamma distribution, two parameters are used defined by beta (shape, β) and alpha (scale, α):

$$g(\tau) = \frac{\Gamma^{\alpha-1}}{\beta^\alpha \Gamma(\alpha)} \exp\left(-\tau/\beta\right) \quad (4)$$

The two other models, exponential and power law, only use one shape parameter. Both models were proven to be ineffective at drastically improving model δQ data compared to the gamma distribution, therefore, they will not be discussed further.

Based on the shortest period of isotope data observations, a maximum of 2190 days (=6 years) into the past was used to evaluate the MTT. However, the gamma distribution model parameters (α and β) were bound such that at least 50% of the gamma PDF fell within the 2190-day analysis period. This allowed us to vary the range of the shape and scale parameters by considering how much of the gamma PDF falls within the data records for each site. The defined gamma convolution model parameters were fit to maximize the model δQ data based on the Kling-Gupta Efficiency (KGE) value closest to 1 (Gupta et al., 2009). The KGE is a model fitness metric that incorporates the correlation coefficient, the bias, and the normalized standard deviation (Knoben et al., 2019). By using the ensemble of 100 daily δP time series, we estimated 100 different MTTs with associated KGE and model parameters. For each ensemble, a global optimization using *scipy.optimize (differential evolution)* was used to find the best gamma model fit with the highest KGE (closest to 1) per NEON site (Virtanen et al., 2020). We utilized other optimizations (that gave bad results) through *scipy.optimize* such as: *basinhoppinh*, *brute*, *shgo*, and *dual annealing*. The chosen optimization, *differential evolution*, uses the three parameters, α, β, and the effective fractionation factor (E_{eff}). E_{eff} is used to account for isotope fractionation. We use the bounds for each parameter respectively of 0.001 to 10^{10}, 0.001 to 10^{10}, and −100 to 100. We used a random seed, 300 iterations, and an initial condition for the function at 1, 365, and 0 for the three parameters respectively. The optimization function allowed us to minimize the gamma model output errors in δQ and search for the best combination of model parameters (α and β) that have the highest KGE.

3 | RESULTS

3.1 | δQ and $\overline{\delta P}$ relation to LMWLs and LSWLs

In this study, we present the NEON stable water isotope data and associated LMWLs and LSWLs across the 26 sites (Figure 2, Table 3). We utilize both stable water isotopes ($\delta^{18}O$ and δ^2H) and associated linear fits (LMWL and LSWL) to understand evaporative and elevation effects at each NEON site. Across all sites, the $\delta^{18}O$ values of precipitation range from −28.4‰ to 13.2‰ and the δ^2H values ranged from −230.4‰ to 21.7‰. The median of the weighted $\overline{\delta^{18}O}$ in precipitation ranges from −17.8‰ to −2.9‰ with an average of −8.4‰ (Table 3). The median of the weighted $\overline{\delta^2H}$ in precipitation ranges from −147.5‰ to −11.8‰ with an average of −59.5‰ (Table 3).

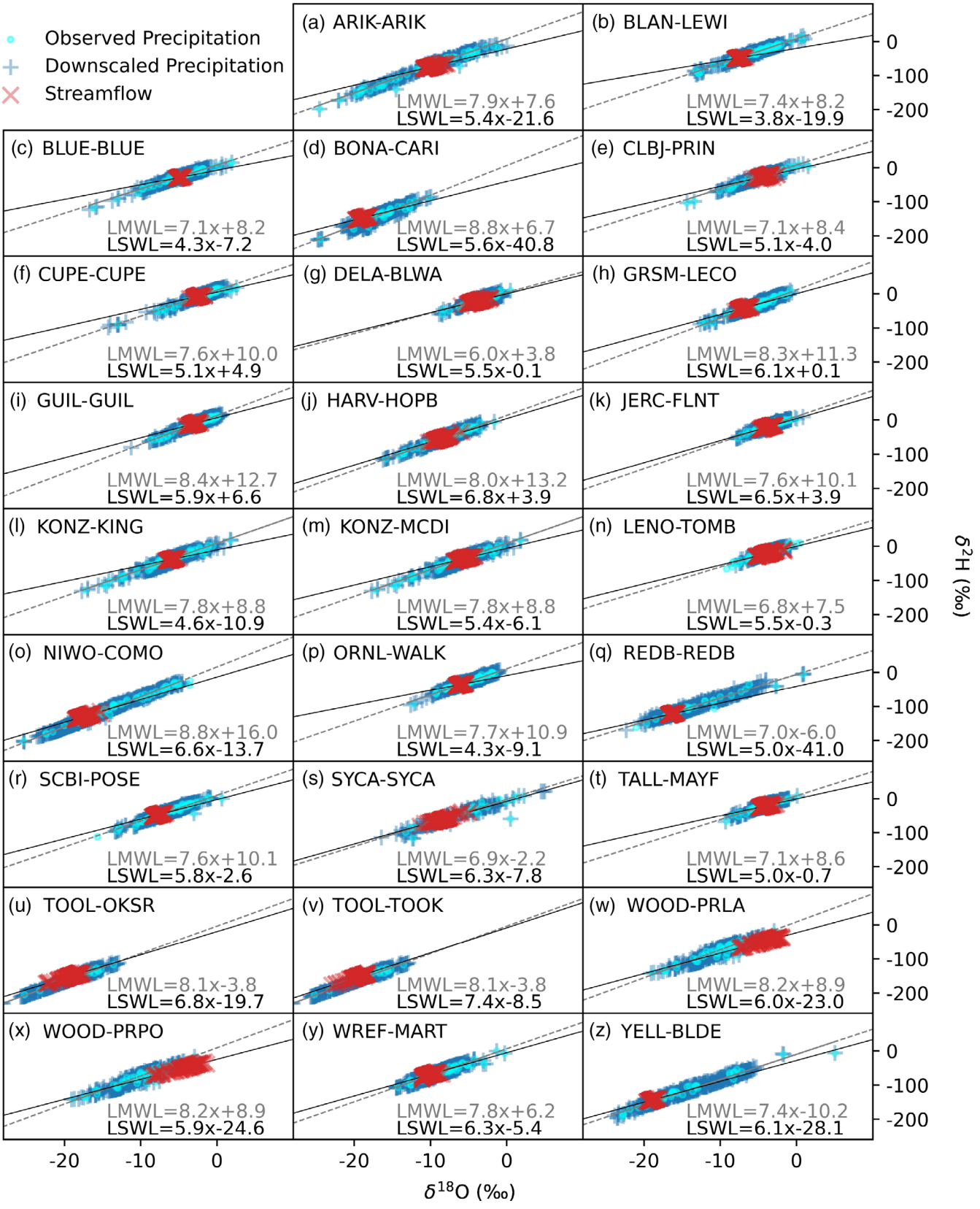

FIGURE 2 Weighted Local Meteoric Water Line (LMWL, solid black line) and unweighted Local Stream water Line (LSWL, dashed grey line) for δ^2H and $\delta^{18}O$ isotopes at National Ecological Observatory Network (NEON) site pairs (lettered a–z). Observed precipitation isotope ratios (cyan) are used with precipitation amounts to create downscaled precipitation isotope values (blue) and are shown with measures of stream water isotope ratios (red). Site names are in Table 1.

Across all sites and samples, the $\delta^{18}O$ values of stream water range from −23.0‰ to −1.4‰ and the $\delta^{2}H$ values ranged from −176.4‰ to −3.6‰. The median of $\delta^{18}O$ in stream water ranges from −19.5‰ to −2.7‰ with an average of −8.7‰ (Table 3). The median of $\delta^{2}H$ ranges from −150.7‰ to −8.3‰ with an average of −61.5‰ (Table 3). Generally, the weighted LMWL has a slope around 8 (mean of 7.7 with standard deviation of 0.6) and the LSWL has a shallower slope (mean of 5.7 with standard deviation of 0.9). The shallower the LSWL slope, the more evaporative effects at that site.

We conducted a brief analysis on the line conditioned excess (*lc-excess*) to understand the evaporative and elevation influences within the δP and δQ data (Landwehr & Coplen, 2006). The *lc-excess* defines the offset between the LMWL and LSWL with a value of 0 indicating no difference between surface water and precipitation water samples (Landwehr & Coplen, 2006). The average *lc-excess* among NEON sites was −0.37‰, which indicates δQ is higher than δP, partially due to evaporation effects.

Several sites show the range of δQ not centred on a majority of the δP observations. This is observed in sites BONI-CARI (d), NIWO-COMO (o), WOOD-PRLA (w), WOOD-PRPO (x), and YELL-BLDE (z) (Figure 2). The sites TOOL-OKSR (u) and TOOL-TOOK (v) show the most negative δQ and δP. These sites show larger spreads in δQ as well as a more negative δQ compared to δP, with positive values of *lc-excess* (in a brief analysis not shown). These sites also show more negative δP observations that are associated with snowfall as the stations are in Alaska (d, u, and v), the Rocky Mountains in Colorado (o), North Dakota (w and x), and in Wyoming (z).

3.2 | Isotope seasonality and F_{yw} estimates

Seasonal patterns in δP and δQ are evident in the NEON stream water samples based on the median of the 100 ensemble-member best wave fits using Equations (2a) and (2b) (Figure 3). Given the strong correlation between $\delta^{18}O$ and $\delta^{2}H$ (Figure 2), only $\delta^{18}O$ was used in the modelling of F_{yw} and MTT. Note that each site's isotope data record begins at different times, which ranges from 2014 to 2018, and continues through the fall of 2022 (Figure 3). The A_P ranges from 0.34‰ to 6.38‰ with an average of 2.78‰ and the A_Q ranges from 0.03‰ to 2.02‰ with an average of 0.4‰ (Table 3).

The relative strength of seasonal amplitudes of δP and δQ values at NEON site determines the amount of young water, F_{yw}, within each location (Figure 4). The average F_{yw} across NEON is 0.20 or 20% of young water and the average standard deviation is 0.02 or 2%. The F_{yw} ranges from 0.01 to 0.93 with about 75% of sites having a F_{yw} less than 0.20 (Table 4).

3.3 | MTT estimates

MTT estimates show a wide range in water transport time throughout the NEON sites (Figure 5, Table 4). The median MTT ranges from 0.1 to 13.2 years with a median of 1.6 years. The median standard deviation ranges from 0.1 to 21.2 years with a median of 1.4 years. The maximum MTT and standard deviations are associated with station ARIK-ARIK (a) and are likely unrealistic and corresponding to one of the lowest KGE model fit of 0.20. The KGE scores range from 0.00 to 0.78 with half of them above 0.47 (Table 4). The diverse range of the gamma model fits and associated KGE scores provide a complex set of results with both confident (high KGE) MTT estimates and inaccurate estimates (low KGE).

The parameters of the gamma function (α and β) vary throughout the NEON sites (Table 4). The α ranges from 0.3 to 12.2 with a median of 0.9 and the β ranges from 0.03 years to 34.30 years with a median of 1.50 years. The ranges of median α and β with the corresponding MTT product in relation to color coded KGE, show no correlation (Figure 6).

The ensemble of downscaled precipitation isotopes allowed the F_{yw} and the gamma model to be run as 100 ensemble-members to obtain estimates of F_{yw} and MTT that incorporate uncertainties in precipitation downscaling. The spread of F_{yw} based on the 100 ensemble-member δP inputs ranges from just above 0.01, site REDB-REDB (q) to above 0.90, site JERC-FLNT (k) (Figure 7). Some estimates of F_{yw} were above 1 and were excluded from analysis due to unrealistic estimates. The largest ensemble spreads of F_{yw} are observed for sites DELA-BLWA (g), JERC-FLNT (k), and LENO-TOMB (n), which corresponds to the largest median F_{yw}. The MTT ensembles range from 0.1 years, site LENO-TOMB (n) to well over 15 years, site ARIK-ARIK (a). As MTT increases, there is a larger spread in the ensemble members. The corresponding median of KGE values range from around 0.00, site BLAN-LEWI (b) to 0.78, site SYCA-SYCA (s). There is no relationship between large spreads or higher median MTT with larger spreads or lower KGE. There should be higher confidence in an MTT estimate when there is a corresponding high median KGE, but also a narrow range of ensemble members. A high KGE and a narrow range of ensemble members shows our model is consistent and accurately models the observed δQ.

4 | DISCUSSION

4.1 | $\overline{\delta P}$ and δQ relation to environment and watershed timescale characteristics

There is variable gamma model performance based on visual model fits from Figure 5 as well as KGE scores from Table 4. Based on this, we utilize select model fits with KGE scores that represent accurate observations of stream water isotopes at NEON sites. We assumed that model fits with a median KGE scores above 0.5 (rounded to nearest tenth) were robust. There were 14 out of 26 NEON sites with a KGE ≥0.5. This KGE threshold is applied to only the gamma model parameters β and α, as well as the output MTT. We choose a rounded KGE of 0.5 because this value includes ensemble spreads that are positive (Figure 7), which are considered strong model fits.

The statistical correlations to be discussed have significant *p*-values ≤0.1 based on a linear regression, with the significance of *p*-

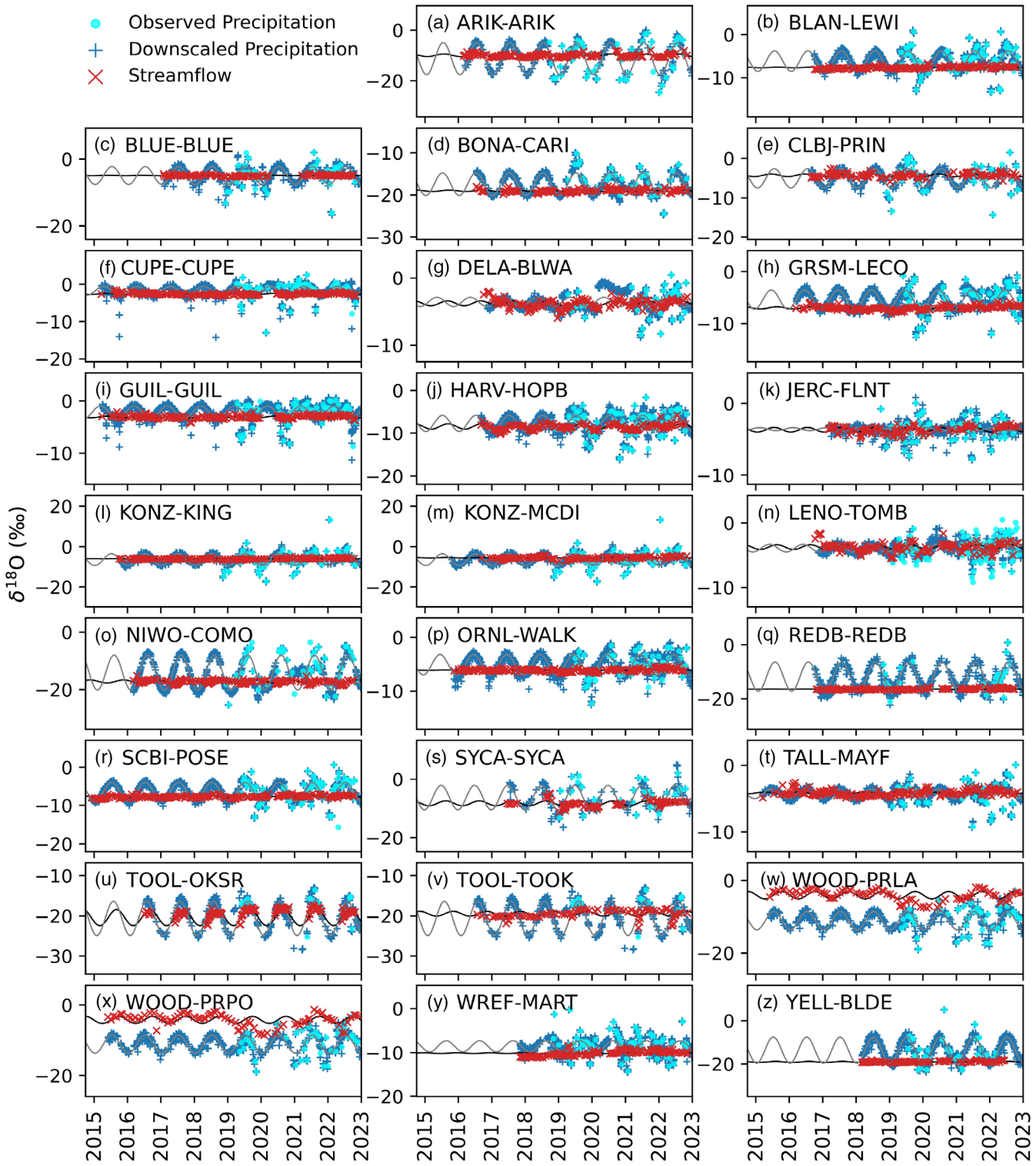

FIGURE 3 Downscaled precipitation isotopes (blue) derived from observed precipitation (cyan) during the stream water (red) sampling period. Best fit sinusoidal curves for precipitation (grey) and stream water (black) for the 26 National Ecological Observatory Network (NEON) site pairs (lettered a–z) from 2014 to 2022. Site names are in Table 1.

value dictating the size of the coloured square in Figure 8. When evaluating the isotope ratios in $\overline{\delta P}$ and δQ across the NEON sites, broad patterns with environmental characteristics are clear (Figure 8a). There are strong positive and negative correlations ($|r| > 0.25$) with the $\delta^{18}O$ and $\delta^{2}H$ median and standard deviation data in $\overline{\delta P}$ and δQ with latitude, longitude, elevation, flow length, clay fraction, silt fraction, temperature, precipitation amount, precipitation intensity, and the precipitation frequency. As NEON sites are further north (i.e., higher

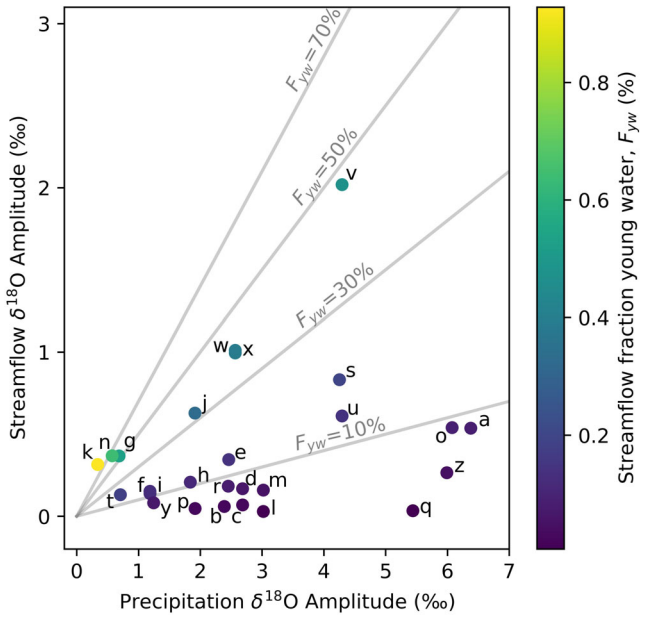

FIGURE 4 Amplitude of precipitation and stream water seasonal variation in δ^{18}O isotope values, with the fraction of young water, F_{yw} (%) denoted by the colour scale. The letters per dot indicate the National Ecological Observatory Network (NEON) site pairs (lettered a–z) and are given in Table 1.

latitude), $\overline{\delta P}$ and δQ become more negative (more depleted, $r = -0.82$), while as NEON sites are further east (i.e., lower longitude) in the continental US and Puerto Rico, $\overline{\delta P}$ and δQ values are more positive (more enriched, $r = -0.83$). There is a negative correlation with the median $\overline{\delta P}$ ($r = -0.6$) and δQ ($r = -0.64$) with NEON site elevation. As NEON sites are located at higher elevation, there is more negative $\overline{\delta P}$ and δQ, and thus the isotope signature is depleted due to the rainout effect. There is a positive correlation with the median $\overline{\delta P}$ ($r = 0.35$) with flow length. It is not clear what processes control NEON sites having longer flow lengths and having more positive $\overline{\delta P}$. There is a positive correlation with the median $\overline{\delta P}$ ($r = 0.45$) and δQ ($r = 0.44$) with the clay fraction, but a negative correlation with the median $\overline{\delta P}$ ($r = 0.41$) with the silt fraction of the NEON site soils. NEON sites that are further north have a lower clay fraction and higher silt fraction, which explains the inverse trend of $\overline{\delta P}$ and δQ with site latitude. NEON sites that are further east have a higher clay fraction and lower silt fraction, which explains the similar trend of $\overline{\delta P}$ and δQ with site longitude. There is a positive correlation with the median $\overline{\delta P}$ ($r = 0.93$) and δQ ($r = 0.85$) with NEON site average temperature, indicating more positive or enriched $\overline{\delta P}$ and δQ NEON with higher average temperature. There is a positive correlation with the median $\overline{\delta P}$ ($r = 0.68$, 0.89) and δQ ($r = 0.58$, 0.85) with NEON site average precipitation and precipitation intensity, indicating more positive $\overline{\delta P}$ and δQ NEON with higher average precipitation and the intensity of precipitation. There is also a positive correlation with the median $\overline{\delta P}$ ($r = 0.36$) with NEON site precipitation frequency. As a NEON site receives more precipitation, the isotope signature is more enriched or positive due to the high amount of precipitation represented in warmer climates (i.e., higher temperatures).

The correlations of $\overline{\delta P}$ and δQ with the NEON watershed characteristics described above are supported by prior continental scale analysis of stream water (Kendall & Coplen, 2001). They showed similar spatial characteristics of δ^{18}O and δ^{2}H across the continental US with more negative isotope ratios in northern latitudes, further western areas, higher elevations, cooler temperatures, and lower precipitation. Kendall & Coplen, 2001 did not weight δP but did discharge weigh δQ observations. Our study showed similar results with unweighted δP vs. weighted $\overline{\delta P}$ observations. The gradient of δ^{18}O and δ^{2}H ratios at higher latitudes and higher elevations are generally depleted due to cooler temperatures and the rainout effect (Allen et al., 2017; Halder et al., 2015). Kendall and Coplen (2001) show the isotope relation to climate parameters in stream water but go on to use the river samples as a proxy for precipitation compositions. They validate δQ data with the adjacent δP data to demonstrate similar correlations to climate parameters and spatial distributions. Kendall and Coplen (2001) show the ranges and spatial distributions of the slope of the LSWL within the range of 5–6‰ with locally higher and lower slopes, which supports the NEON average LSWL slope of 5.7‰. There are lower slopes in western and further north sites, which imply enhanced evaporation effects, partly due to snow sublimation for northern sites. This is supported by Beria et al., 2018, which reviewed the state of the knowledge in relation to how different hydrometeorological processes affect the isotopic composition of snow in its different forms (snowfall, snowpack, and snowmelt).

The seasonal cycles of δ^{18}O in precipitation (A_P) and stream water (A_Q) show a correlation, both positive and negative ($|r| \geq 0.25$) with latitude, longitude, elevation, temperature, precipitation, precipitation intensity, and precipitation frequency (Figure 8a). The A_P and A_Q increase with further north NEON sites. The A_P and A_Q decrease as NEON sites are further east in the continental US and Puerto Rico, lower elevated, warmer temperatures, higher precipitation, and higher precipitation intensity. The A_P shows an additional positive correlation ($r = 0.83$) with the average watershed elevation. This is supported through the median values of δ^{18}O and δ^{2}H in precipitation mentioned earlier. Halder et al. (2015) showed the average seasonal amplitude of δ^{18}O in stream water to be 2.5‰ and precipitation to 7.5‰ across the globe. More than half of seasonal δ^{18}O amplitudes in stream water were below 2.0‰, which is closer to our average of 0.4‰ (Halder et al., 2015). Halder et al. (2015) studied global rivers and did geographically separate results, but our results are a fraction of the sample size in comparison, so it is reasonable to show that the A_P and A_Q in δ^{18}O relationships are different than Halder et al. (2015). Despite the differences in quantitate values, Halder et al. (2015) did show a strong correlation between the amplitude as a function of latitude in δP but not δQ. We show a slightly stronger correlation with δQ ($r = 0.52$) than δP ($r = 0.42$). This difference might be due to the difference in global versus North American study sites. Halder et al. (2015) showed a similar lack of correlation with watershed areas.

TABLE 4 The fraction of young water, (F_{yw}) and mean transit time (MTT) characteristics between 100 ensemble-member model runs at each National Ecological Observatory (NEON) site pairs (lettered a–z).

Precip-stream	F_{yw}	β	α	MTT	KGE
	Median (Std)	Median (Std)	Median (Std)	Median (Std)	Median (Std)
(a) ARIK-ARIK	0.08 (0.00)	34.3 (8.4)	0.4 (0.1)	13.2 (21.2)	0.20 (0.04)
(b) BLAN-LEWI	0.02 (0.00)	4.5 (6.3)	0.6 (1.6)	2.8 (3.5)	0.00 (0.06)
(c) BLUE-BLUE	0.03 (0.00)	4.7 (2.5)	1.5 (0.7)	7.1 (5.7)	0.33 (0.26)
(d) BONA-CARI	0.06 (0.00)	0.5 (0.1)	3.4 (0.4)	1.8 (1.0)	0.30 (0.00)
(e) CLBJ-PRIN	0.14 (0.01)	20.8 (16.2)	0.3 (0.1)	5.8 (11.0)	0.23 (0.19)
(f) CUPE-CUPE	0.12 (0.01)	8.3 (4.0)	0.7 (0.9)	5.7 (7.0)	0.68 (0.07)
(g) DELA-BLWA	0.54 (0.07)	1.0 (0.5)	0.7 (0.1)	0.8 (0.9)	0.26 (0.02)
(h) GRSM-LECO	0.11 (0.01)	5.6 (2.8)	0.6 (0.0)	3.3 (4.4)	0.68 (0.02)
(i) GUIL-GUIL	0.13 (0.01)	16.4 (4.1)	0.6 (0.0)	9 (12.1)	0.61 (0.02)
(j) HARV-HOPB	0.33 (0.02)	0.4 (0.1)	0.9 (0.1)	0.4 (0.4)	0.74 (0.01)
(k) JERC-FLNT	0.93 (0.08)	0.1 (0.1)	5.4 (24)	0.5 (0.2)	0.38 (0.19)
(l) KONZ-MCDI	0.01 (0.00)	0.3 (0.5)	3.9 (5.2)	1.4 (0.6)	0.56 (0.09)
(m) KONZ-KING	0.05 (0.00)	0.2 (0.3)	3.9 (5.1)	0.7 (0.4)	0.47 (0.11)
(n) LENO-TOMB	0.64 (0.05)	0.1 (0.3)	0.9 (0.7)	0.1 (0.1)	0.65 (0.03)
(o) NIWO-COMO	0.09 (0.00)	1.6 (0.4)	0.9 (0.1)	1.4 (1.5)	0.20 (0.03)
(p) ORNL-WALK	0.02 (0.00)	15.6 (3.7)	0.6 (0.0)	9.0 (11.9)	0.58 (0.02)
(q) REDB-REDB	0.01 (0.00)	1.0 (0.9)	5.3 (3.4)	5.5 (2.4)	0.38 (0.08)
(r) SCBI-POSE	0.07 (0.00)	4.3 (2.1)	0.7 (0.1)	3.0 (3.6)	0.28 (0.03)
(s) SYCA-SYCA	0.20 (0.01)	1.5 (0.5)	0.9 (0.1)	1.3 (1.4)	0.78 (0.03)
(t) TALL-MAYF	0.19 (0.02)	9.3 (7.6)	0.3 (0.1)	2.7 (5.1)	0.27 (0.08)
(u) TOOL-OKSR	0.47 (0.02)	2.1 (1.3)	0.4 (0.1)	0.9 (1.3)	0.47 (0.08)
(v) TOOL-TOOK	0.14 (0.01)	0.4 (0.1)	0.9 (0.1)	0.4 (0.4)	0.57 (0.05)
(w) WOOD-PRLA	0.39 (0.03)	0.1 (0.0)	5.1 (0.9)	0.3 (0.2)	0.55 (0.04)
(x) WOOD-PRPO	0.39 (0.03)	0.0 (0.0)	12.2 (6.6)	0.3 (0.1)	0.46 (0.05)
(y) WREF-MART	0.07 (0.01)	0.2 (0.0)	3.6 (0.5)	0.7 (0.3)	0.53 (0.04)
(z) YELL-BLDE	0.04 (0.00)	11.4 (2.5)	0.8 (0.6)	8.9 (10.1)	0.13 (0.14)

Note: The median and standard deviation (Std) of F_{yw}, median beta (β–scale), alpha (α–shape) MTT, and Kling-Gupta Efficiency (KGE).

The relationship between Tables 3 and 4 of the isotope characteristics of $\overline{\delta P}$ and δQ with the watershed timescale metrics show some correlations across characteristics (Figure 8b). There is a positive correlation with the median of $\overline{\delta P}$ and the median of F_{yw} ($r = 0.16$). There is a negative correlation with the standard deviation of $\overline{\delta P}$ and the median of F_{yw} ($r = -0.19$), β ($r = -0.51$), median MTT ($r = -0.56$), and the standard deviation of the MTT ($r = -0.53$). There is a positive correlation with the median of δQ and the standard deviation of F_{yw} ($r = 0.37$). There are also correlations with the standard deviation of δQ and the median F_{yw} ($r = 0.44$), β ($r = -0.56$), α ($r = 0.58$), median MTT ($r = -0.61$), and the standard deviation of MTT ($r = -0.58$). There are other correlations, some of which seem spurious, between the slope of the LSWL with the standard deviation of F_{yw}, the slope and intercept of the LSWL with the F_{yw} and other timescale metrics. Finally, there is a negative correlation between the A_P and the median as well as standard deviation of the F_{yw} ($r = -0.43, -0.52$). As the amplitude becomes larger, the F_{yw} becomes smaller.

4.2 | Watershed timescale metrics' relation to environmental characteristics and themselves

Watershed timescale metrics and environmental characteristics estimated in this study show some correlations (Figure 8c) denoting local controls over watershed hydrology. There is a positive correlation between the median ($r = 0.61$) of the F_{yw} and the watershed area. As the watershed becomes larger, the F_{yw} becomes higher. There is also a positive correlation between the median ($r = 0.76, 0.63$) of the F_{yw} and the flow length and the flow length/slope. As the watershed becomes larger with a longer flow length, the F_{yw} becomes higher. Lutz et al. (2018) found non-significant correlations between F_{yw} and a wide range of watershed characteristics for mean watershed slope, median flow path length, watershed area, soil fractions of sand, silt, and clay. Despite that, they did find a correlation between F_{yw} and annual precipitation (Lutz et al., 2018). von Freyberg et al. (2018) also showed a positive correlation between the F_{yw} and the mean monthly

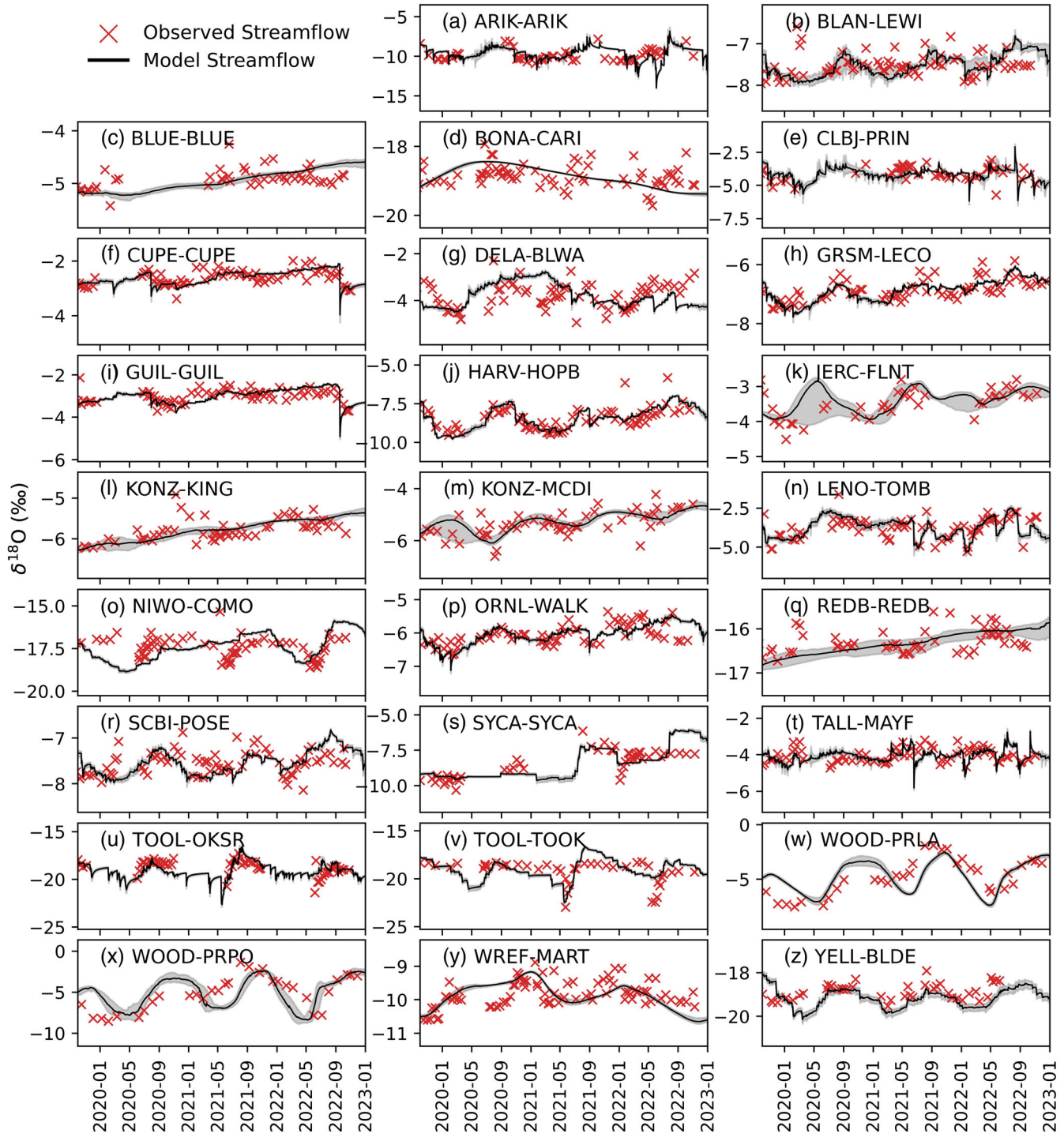

FIGURE 5 The gamma convolution model fit of $\delta^{18}O$ stream water isotopes (black line) compared against observed stream water isotopes (red 'x') per National Ecological Observatory Network (NEON) site pairs (lettered a–z). The grey shading is the inter quartile range of the model fit between the 100 ensemble-member model runs. The model analysis statistics per site pair are in Table 4. Site names are in Table 1.

precipitation, mean precipitation intensity, and drainage density. They show a weak negative correlation with watershed area, but a strong negative correlation when they omit high-elevation snow-dominated sites (von Freyberg et al., 2018). When we omit the five snow-dominated sites, the correlations do not change significantly. Jasechko et al. (2016) showed no significant correlations between the F_{yw} and watershed size and annual precipitation for additional reference.

We did not weigh δQ based on stream water because of limitations with NEON discharge data (Rhea et al., 2023). von Freyberg et al. (2018) showed that flow weighting the δQ yielded F_{yw} that was

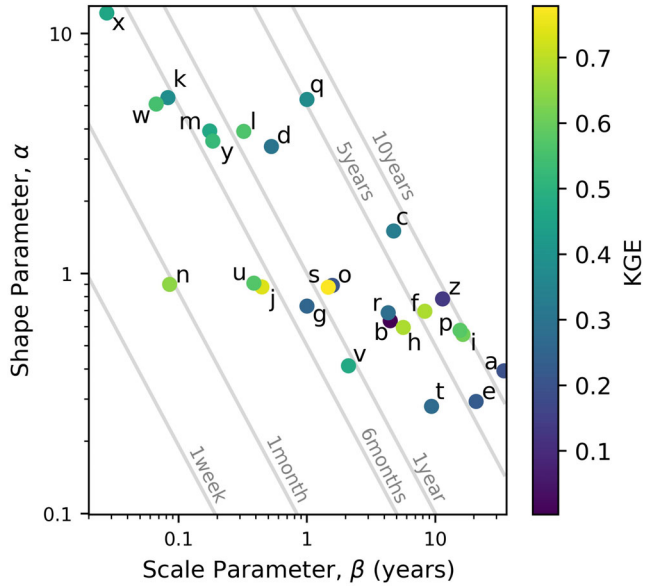

FIGURE 6 The median alpha (α–shape) and beta (β–scale) parameters on a logarithmic scale used to calculate the gamma convolution model color coded by median Kling-Gupta efficiency (KGE) per National Ecological Observatory Network (NEON) site pairs (lettered a–z). The product of α and β is the mean transit time, highlighted by the grey lines, which is also in Table 4. Site names are in Table 1.

roughly 26% larger than their unweighted counterparts F_{yw}, but Segura (2021) found indistinguishable results considering weighted or unweighted output signals in the F_{yw} estimates. von Freyberg et al. (2018) studied watersheds in Switzerland that were sized 0.7–351 km^2 while Segura (2021) studied watersheds in the Oregon Cascades that were sized 0.2–64 km^2. Our study analyzed watershed sizes from 1 to 47 085 km^2.

There are correlations between β and latitude ($r = -0.54$), longitude ($r = 0.49$), slope ($r = 0.65$), clay fraction ($r = 0.61$), and precipitation frequency ($r = 0.71$) (Figure 8c). There are correlations between α and sand fraction ($r = -0.47$), silt fraction ($r = 0.69$), and porosity ($r = 0.54$). Hrachowitz et al. (2010) showed the β was controlled by precipitation intensities, supporting our observation, consistent with Lutz et al. (2018). Hrachowitz et al. (2010) also showed that α has no relationship with precipitation intensity but was found to be closely related to watershed landscape organization, notably the hydrological characteristics of the dominant soils and the drainage density, consistent with Lutz et al. (2018). This is supported with α correlations to sand fraction, silt fraction, and the soil porosity. The impacts on the large range in α and β on MTT estimates observed in this study are shown to be primarily controlled by soil and precipitation characteristics, supported by past studies (Hrachowitz et al., 2010; Lutz et al., 2018).

There are correlations between the median and standard deviation of the MTT with latitude ($r = -0.58$), longitude ($r = 0.52$), slope ($r = 0.68$), clay fraction ($r = 0.62$), precipitation ($r = 0.48$), and precipitation frequency ($r = 0.71$) (Figure 8c). There is also a correlation between the median MTT and temperature ($r = 0.49$). The transit time of water gets shorter as NEON sites are further north. The transit time of water gets longer as NEON sites are further east among our sites in the continental US and Puerto Rico. The transit time of water gets longer as NEON sites have steeper slopes, higher clay fraction, warmer temperatures, more precipitation, and a higher precipitation frequency. These results show NEON site water age is primarily determined by the site location within the continental US and Puerto Rico, gradient (slope), soil characteristics, and climate characteristics. Other studies have shown several similar and different relationships between MTT and environmental characteristics (Capell et al., 2012; Clow et al., 2018; Gabrielli & McDonnell, 2020; Lutz et al., 2018; Maxwell et al., 2016; McGuire et al., 2005; Mosquera et al., 2016; Segura, 2021). Each of these studies was conducted in smaller geographic areas and not over a large scale like our study. Clow et al. (2018) showed relationships to topographic and geologic characteristics in mountain watersheds of the western US, whereas the Jasechko et al. (2016) study found different relationships over agricultural areas. Gabrielli and McDonnell (2020) showed a relationship between geology, landscape structure, and water transit times within the critical zone of eight diverse geologic watersheds with similar rainfall, thin soils, and steep slopes. They go on to acknowledge their conclusions would be less likely to show trends with MTT in climates with less precipitation or higher evaporation (Gabrielli & McDonnell, 2020). Segura (2021) showed that wet and dry years contribute to relationships of MTT and F_{yw} with watershed characteristics differently. For example, the MTT was negatively correlated to drainage area in a non-drought year and unrelated to drainage area during a drought year (Segura, 2021). The F_{yw} was positively correlated to drainage area in a drought year but unrelated in all other years, including other drought years (Segura, 2021). The inconsistent relations of MTT and F_{yw} correlations to environmental characteristics show the diverse nature of water transport processes and the times. Finally, there is a correlation between KGE and slope ($r = 0.37$) of the watershed (Figure 8c). As KGE increases, there is a steeper slope. Our gamma model based on optimization works best for watersheds with steeper slopes. This might make sense as water moves quicker through various environments, our model can work better. However, we do not observe shorter MTT with steeper watersheds, therefore it is unclear why we have a positive correlation with KGE and slope.

Figure 8d shows whether any watershed timescale metrics are related to each other. Visually from Figure 7, there were longer median MTT with lower F_{yw}, which is supported by a negative correlation ($r = -0.46$). The MTT and F_{yw} relationship is supported by Lutz et al. (2018), which found larger F_{yw} tended to have predominantly short transit times and thus a rapid response to solute input in stream water.

4.3 | Understanding water ages across NEON

MTT and F_{yw} have been previously studied across a wide range of environments to synthesize consistent correlations to water transport

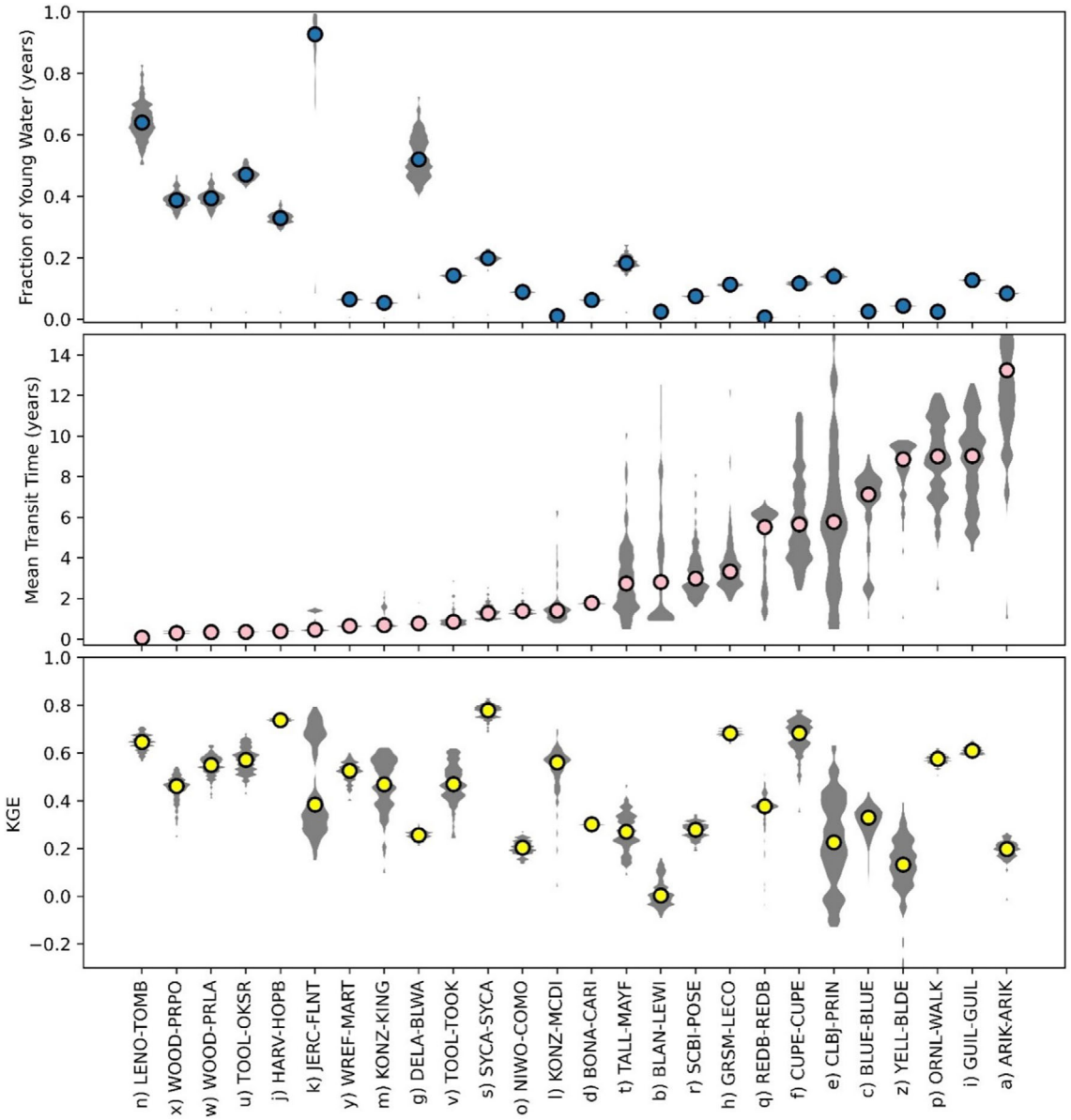

FIGURE 7 The 100 ensemble-member gamma convolution model results of fraction of young water (top), mean transit time (MTT) (middle), and Kling-Gupta efficiency (KGE) (bottom) per National Ecological Observatory Network (NEON) site pairs (lettered a–z). The sites are arranged from lowest median MTT to the highest with NEON site pairs labelled. The coloured circles per plot indicate the median value for that site pair.

processes, yet the diversity of the spatial and temporal data used makes it difficult to ascertain consistent results. This is because these studies use a wide range of data sources with varying amounts of incoming precipitation measurements (both isotope ratios and amount) and outgoing discharge (both isotope ratios and volume) (Bansah & Ali, 2019; Benettin et al., 2017; Capell et al., 2012; Gabrielli & McDonnell, 2020; McGuire et al., 2005; Mosquera et al., 2016; Segura, 2021; Stockinger et al., 2016; van Meerveld et al., 2019; von Freyberg et al., 2018). The data used are often from small areas, with limits on the amount of data collected temporally and spatially (Capell et al., 2012). This can lead to temporal and spatial limits on MTT and F_{yw} calculations, and potentially cause errors or misleading estimates (Stockinger et al., 2016). The differences in sampling frequency and spatial variability of collected observations specific in the prior studies potentially create limitations to understanding spatial variability of water transport timescales. However, in this study with consistent data collection and analysis approaches, we still find a diverse range of water ages across NEON with some correlations to environmental characteristics. This suggests that MTT and F_{yw} are determined by a combination of complex local factors.

The median MTT across the 100 ensemble-member ranges from a couple of months to over 13 years (Figure 7, Table 4). There is varying confidence with these estimates based on our model fits against observations using the KGE. Over half of the sites have median KGE scores above 0.30 (Table 4). When we use a KGE threshold of ≥0.5, the MTT ranges from a couple of months to 9 years. The KGE

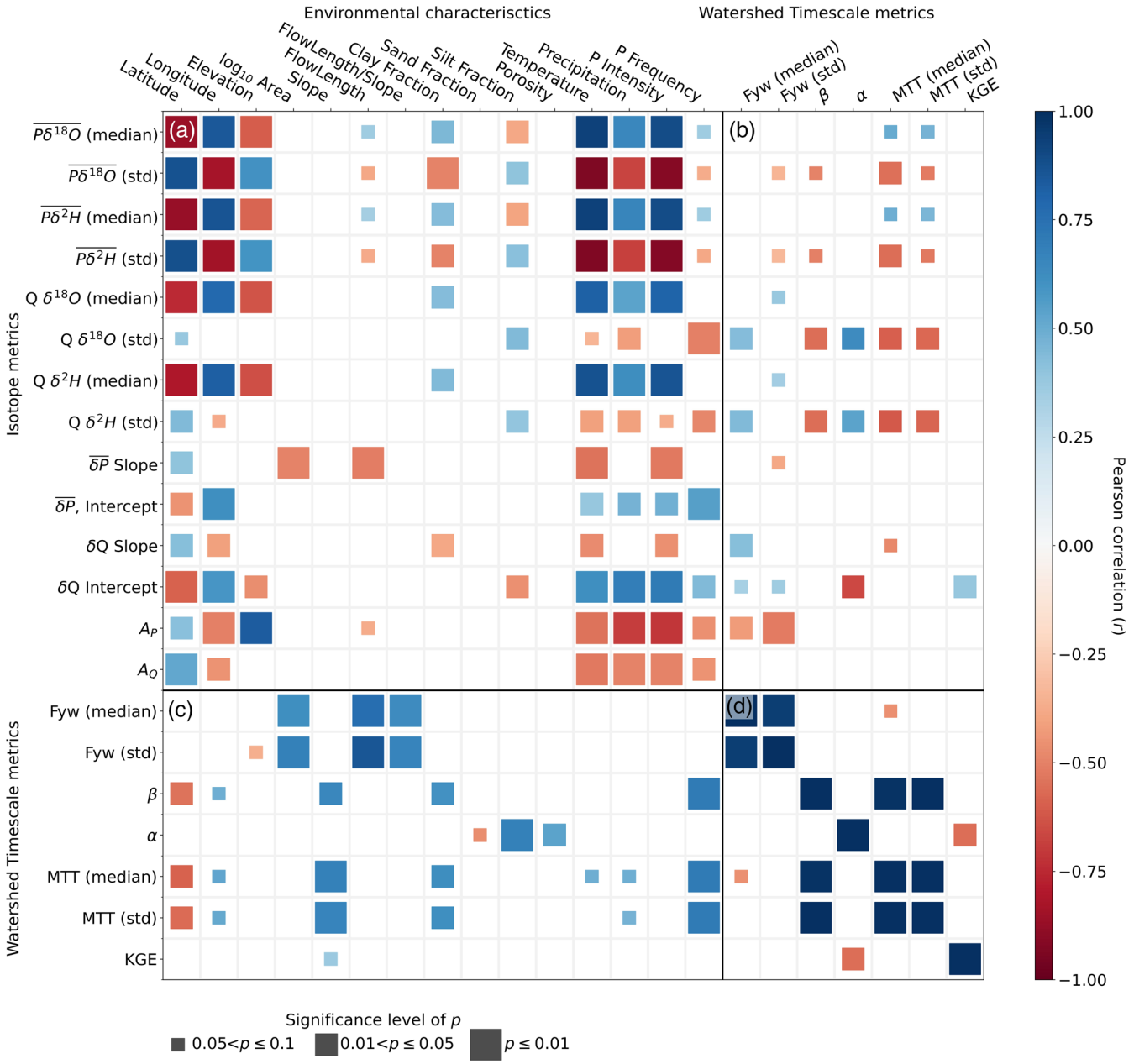

FIGURE 8 Pearson correlation between environmental characteristics (from Tables 1 and 2) vs. calculated isotope metrics (from Table 3) and vs. watershed timescale results (from Table 4). Pearson correlation (r) values are coloured based on the strength of the relationship, with the size of the colour block is based on the significance level of a linear regression with the p-value (p) as described in plot footnote. Block A is Tables 1 and 2 (environmental characteristics) vs. Table 3 (isotope metrics). Block B is Table 3 (isotope metrics) vs. Table 4 (watershed timescale metrics). Block C is Table 4 (watershed timescale metrics) vs. Tables 1 and 2 (environmental characteristics). Block D is Table 4 vs. Table 4.

threshold allows us to consider strong model fits when considering correlations between MTT, α, and β. When the F_{yw} and MTT have small ranges with a narrow and positive KGE range, this supports consistent model performance, such as sites HARV-HOPB (j), SYCA-SYCA (s), and WREF-MART (y) (Figure 7). Sites with negative KGE values and large ranges in MTT should be carefully analysed and understood due to potential model errors, such as sites BLAN-LEWI (b), CLBJ-PRIN (e), and YELL-BLDE (z). Sites that show MTT longer than 6 years are often correlated with poor KGE or large ranges in MTT (Figure 7). This is because NEON sites have, at this point, a maximum of 6 years of δP and δQ data. We can estimate MTT longer than 6 years because we include a wide range of α and β. We do this to include possibilities of small or large α and β. It should be noted that MTT longer than 6 years should be understood with greater uncertainty. Lutz et al. (2018) showed that MTT values above 60 months (5 years) should be considered cautiously, as strong damping of stable water isotope ratios in stream water complicates the determination of MTTs of above 5 years.

4.4 | Sources of uncertainty and limitations

There are several sources of uncertainty and limitations derived from both the data available and methods used. Since we only have one precipitation measurement location at each NEON site, elevation effects on the isotope concentration were not considered. A maximum distance of 20 km was used to ensure precipitation isotope ratios reflected the same precipitation that would affect residence times and stream water isotope ratios. Most sites were within 5 km, but several were outside this distance. The distance between precipitation and stream measurement did not correlate to KGE or other model values. For the larger watersheds we analysed (>50 km) which consisted of ~35% of the NEON sites, the precipitation measurement is still within 20 km of the aquatic measurement. The large watersheds (except LENO-TOMB (n)) do not have other precipitation measurements, that might be more representative of upstream characteristics. As mentioned earlier, we average the $\overline{\delta P}$ and precipitation observations for LENO-TOMB (n), which encompasses the nested watersheds DELA-BLWA (g) and TALL-MAYF (t). Future work to further understand large scale watersheds transport times would need to consider δP isoscapes, in part using isotope modelling, that would be representative of the larger watershed inputs (Waterisotopes.org, 2023; Yoshimura et al., 2008).

Snow related isotope processes (i.e., sublimation) can have important effects on isotope composition (Beria et al., 2018). We account for snowpack fractionation using E_{eff} in our gamma model. We do not account for other snowpack processes (i.e., melting, spatial distribution) and the potential impact that snow has on the composition of δP and δQ over a watershed. Despite that, we observed potential snowpack effects on isotope composition at several sites (d, o, u, v, w, x, and z). These sites as mentioned earlier showed more negative δQ compared to δP, with positive values of *lc-excess*. At these sites, precipitation over the catchment is likely not represented by the gauge collecting δP. Snow falling at higher elevations compared to the δP tower collection site would be more negative than the tower, so the δQ (derived from snow) would be more negative than the δP that we observe.

The δP and δQ data show seasonality and suggest a possibly time varying residence time distribution. A flow-corrected time based on daily discharge similar to McGuire et al. (2005) did not improve MTT calculations, in part due to the limitations of discharge data (Rhea et al., 2023). Additionally, StorAge Selection (SAS) functions were not possible with the limitations of discharge data (Benettin et al., 2017; Rhea et al., 2023). This time invariant MTT presented here needs to be considered with our results but should be noted that McGuire et al. (2005) and Kirchner et al. (2001) included discharge changes in MTT and obtained similar fits to the stream isotope data.

5 | CONCLUSIONS

The co-located δP and δQ across 26 NEON sites provide a unique dataset in the continental US and Puerto Rico to understand watershed processes and the time it takes water to move through NEON study sites. The data is available at varying time periods beginning from 2014 to 2018 but continues through the present as NEON continues to gather data for the foreseeable future. The data presented with Finkenbiner et al. (2021) statistical downscaling of δP and using the NEON-DICEE Dataset allows additional data to understand hydrologic processes with the methods we use. Using the δP and δQ available at 26 NEON sites we can estimate F_{yw} and MTT with varying levels of confidence based on MTT KGE scores. The F_{yw} varies across NEON with from 1% to 93% with a majority less than 20%. We are not able to weigh the F_{yw} based on discharge values due to NEON data limits. The MTT varies from 0.1 to 13.2 years with a median of 1.6 years with half of the sites having a MTT shorter than 2 years. Some MTT have large ranges when using the 100 ensemble-members of the gamma convolution model. The associated KGE gives confidence in the model fit when they are positive with small ranges, which occurs at several sites. Using isotope metrics, watershed timescale metrics, and environmental characteristics shows statistically significant correlations throughout the continental US and Puerto Rico. Isotope metrics of the $\overline{\delta P}$ and δQ data show documented correlations to environmental characteristics in addition to the LMWL and LSWL. The watershed timescale metrics show some documented correlations to environmental characteristics, all be it not as clear as what past studies have shown. This indicates it is difficult to correlate consistent climate, geographic, and geomorphic variables to F_{yw} and MTT properties across the continental US and Puerto Rico. This is due to the complex processes that affect water movement, which vary on different temporal and spatial scales. Several limitations and uncertainties need to be considered with our approach, but do not discount the results shown. The uniqueness of NEON and data availability provides a powerful source to understand hydrologic processes by linking surface and subsurface processes in various ecosystems throughout the continental US and Puerto Rico. NEON sites have a wealth of environmental observations and research that analyses biodiversity and forest ecosystems such as information about plants, animals, soil, nutrients, freshwater, and the atmosphere (Goodman et al., 2015; NEON, 2023b). The isotope data presented here using the LMWL, LSWL, F_{yw}, and MTT can help constrain and provide insight into a variety of water related processes and sciences within NEON study sites.

ACKNOWLEDGEMENTS

This study was funded by the National Science Foundation (NSF), Grant/Award Numbers: 1802885, 1836768, and 1943574. Hu is supported by the U.S. Department of Energy Office of Science BER as part of the BER's Environmental System Science (ESS) program, by the project of River Corridor Science Focus Area. We thank the National Ecological Observatory Network and their support staff for assistance in interpreting and downloading data products. I thank Renee Brooks from the Environmental Protection Agency for the helpful discussions.

DATA AVAILABILITY STATEMENT

NEON isotopes in precipitation and stream water data were provided from NEON's Data Portal, which is a project sponsored by the NSF

and managed under cooperative agreement by NEON, Inc. NEON-DICEE downscaling of precipitation is isotopes is available at https://doi.org/10.4211/hs.e74edc35d45441579d51286ea01b519f.

ORCID

Zachariah Butler https://orcid.org/0009-0007-0883-7103
Stephen Good https://orcid.org/0000-0003-4363-1577

REFERENCES

Allen, S. T., Keim, R. F., Barnard, H. R., McDonnell, J. J., & Renée Brooks, J. (2017). The role of stable isotopes in understanding rainfall interception processes: A review. *WIREs Water*, *4*(1), 1–17. https://doi.org/10.1002/wat2.1187

Bansah, S., & Ali, G. (2019). Streamwater ages in nested, seasonally cold Canadian watersheds. *Hydrological Processes*, *33*(4), 495–511. https://doi.org/10.1002/hyp.13373

Benettin, P., Soulsby, C., Birkel, C., Tetzlaff, D., Botter, G., & Rinaldo, A. (2017). Using SAS functions and high-resolution isotope data to unravel travel time distributions in headwater catchments. *Water Resources Research*, *53*(3), 1864–1878. https://doi.org/10.1002/2016WR020117

Beria, H., Larsen, J. R., Ceperley, N. C., Michelon, A., Vennemann, T., & Schaefli, B. (2018). Understanding snow hydrological processes through the lens of stable water isotopes. *WIREs Water*, *5*(6), e1311. https://doi.org/10.1002/wat2.1311

Brooks, J. R., Barnard, H. R., Coulombe, R., & McDonnell, J. J. (2010). Ecohydrologic separation of water between trees and streams in a Mediterranean climate. *Nature Geoscience*, *3*(2), 100–104. https://doi.org/10.1038/ngeo722

Brooks, J. R., Gibson, J. J., Birks, S. J., Weber, M. H., Rodecap, K. D., & Stoddard, J. L. (2014). Stable isotope estimates of evaporation: Inflow and water residence time for lakes across the United States as a tool for national lake water quality assessments. *Limnology and Oceanography*, *59*(6), 2150–2165. https://doi.org/10.4319/lo.2014.59.6.2150

Capell, R., Tetzlaff, D., Hartley, A. J., & Soulsby, C. (2012). Linking metrics of hydrological function and transit times to landscape controls in a heterogeneous mesoscale catchment. *Hydrological Processes*, *26*(3), 405–420. https://doi.org/10.1002/hyp.8139

Clow, D. W., Mast, M. A., & Sickman, J. O. (2018). Linking transit times to catchment sensitivity to atmospheric deposition of acidity and nitrogen in mountains of the western United States. *Hydrological Processes*, *32*(16), 2456–2470. https://doi.org/10.1002/hyp.13183

Finkenbiner, C. E., Good, S. P., Allen, S. T., Fiorella, R. P., & Bowen, G. J. (2021). A statistical method for generating temporally downscaled geochemical tracers in precipitation. *Journal of Hydrometeorology*, *22*(10), 1473–1486. https://doi.org/10.1175/JHM-D-20-0142.1

Finkenbiner, C. E., Li, B., Spencer, L., Butler, Z., Haagsma, M., Fiorella, R. P., Allen, S. T., Anderegg, W., Still, C. J., Noone, D., Bowen, G. J., & Good, S. P. (2022). The NEON daily isotopic composition of environmental exchanges dataset. *Scientific Data*, *9*(1), 353. https://doi.org/10.1038/s41597-022-01412-4

Fiorella, R. P., Siler, N., Nusbaumer, J., & Noone, D. C. (2021). Enhancing understanding of the hydrological cycle via pairing of process-oriented and isotope ratio tracers. *Journal of Advances in Modeling Earth Systems*, *13*(10), e2021MS002648. https://doi.org/10.1029/2021MS002648

Gabrielli, C. P., & McDonnell, J. J. (2020). Modifying the Jackson index to quantify the relationship between geology, landscape structure, and water transit time in steep wet headwaters. *Hydrological Processes*, *34*(9), 2139–2150. https://doi.org/10.1002/hyp.13700

Godsey, S. E., Aas, W., Clair, T. A., de Wit, H. A., Fernandez, I. J., Kahl, J. S., Malcolm, I. A., Neal, C., Neal, M., Nelson, S. J., Norton, S. A., Palucis, M. C., Skjelkvåle, B. L., Soulsby, C., Tetzlaff, D., & Kirchner, J. W. (2010). Generality of fractal 1/f scaling in catchment tracer time series, and its implications for catchment travel time distributions. *Hydrological Processes*, *24*(12), 1660–1671. https://doi.org/10.1002/hyp.7677

Good, S. P., Noone, D., & Bowen, G. (2015). Hydrologic connectivity constrains partitioning of global terrestrial water fluxes. *Science*, *349*(6244), 175–177. https://doi.org/10.1126/science.aaa5931

Goodman, K. J., Parker, S. M., Edmonds, J. W., & Zeglin, L. H. (2015). Expanding the scale of aquatic sciences: The role of the National Ecological Observatory Network (NEON). *Freshwater Science*, *34*(1), 377–385. https://doi.org/10.1086/679459

Gupta, H. V., Kling, H., Yilmaz, K. K., & Martinez, G. F. (2009). Decomposition of the mean squared error and NSE performance criteria: Implications for improving hydrological modeling. *Journal of Hydrology*, *377*, 80–91. https://doi.org/10.1016/j.jhydrol.2009.08.003

Halder, J., Terzer, S., Wassenaar, L. I., Araguás-Araguás, L. J., & Aggarwal, P. K. (2015). The global network of isotopes in Rivers (GNIR): Integration of water isotopes in watershed observation and riverine research. *Hydrology and Earth System Sciences*, *19*(8), 3419–3431. https://doi.org/10.5194/hess-19-3419-2015

Hrachowitz, M., Soulsby, C., Tetzlaff, D., Malcolm, I. A., & Schoups, G. (2010). Gamma distribution models for transit time estimation in catchments: Physical interpretation of parameters and implications for time-variant transit time assessment. *Water Resources Research*, *46*(10), 2010WR009148. https://doi.org/10.1029/2010WR009148

Jasechko, S., Kirchner, J. W., Welker, J. M., & McDonnell, J. J. (2016). Substantial proportion of global streamflow less than three months old. *Nature Geoscience*, *9*(2), 126–129. https://doi.org/10.1038/ngeo2636

Kendall, C., & Coplen, T. B. (2001). Distribution of oxygen-18 and deuterium in river waters across the United States. *Hydrological Processes*, *15*(7), 1363–1393. https://doi.org/10.1002/hyp.217

Kirchner, J. W. (2016a). Aggregation in environmental systems – Part 1: Seasonal tracer cycles quantify young water fractions, but not mean transit times, in spatially heterogeneous catchments. *Hydrology and Earth System Sciences*, *20*(1), 279–297. https://doi.org/10.5194/hess-20-279-2016

Kirchner, J. W. (2016b). Aggregation in environmental systems – Part 2: Catchment mean transit times and young water fractions under hydrologic nonstationarity. *Hydrology and Earth System Sciences*, *20*(1), 299–328. https://doi.org/10.5194/hess-20-299-2016

Kirchner, J. W., Feng, X., & Neal, C. (2001). Catchment-scale advection and dispersion as a mechanism for fractal scaling in stream tracer concentrations. *Journal of Hydrology*, *254*(1–4), 82–101. https://doi.org/10.1016/S0022-1694(01)00487-5

Knoben, W. J. M., Freer, J. E., & Woods, R. A. (2019). *Technical note: Inherent benchmark or not? Comparing Nash-Sutcliffe and Kling-Gupta efficiency scores* (preprint). Catchment hydrology/Modelling approaches. https://doi.org/10.5194/hess-2019-327

Landwehr, J. M., & Coplen, T. B. (2006). Line-conditioned excess: A new method for characterizing stable hydrogen and oxygen isotope ratios in hydrologic systems. In *International conference on isotopes in environmental studies* (pp. 132–135). IAEA Vienna.

Lutz, S. R., Krieg, R., Müller, C., Zink, M., Knöller, K., Samaniego, L., & Merz, R. (2018). Spatial patterns of water age: Using young water fractions to improve the characterization of transit times in contrasting catchments. *Water Resources Research*, *54*(7), 4767–4784. https://doi.org/10.1029/2017WR022216

Maloszewski, P., & Zuber, A. (1982). Determining the turnover time of groundwater systems with the aid of environmental tracers. Models and their applicability. *Journal of Hydrology*, *57*, 207–231. https://doi.org/10.1016/0022-1694(82)90147-0

Maxwell, R. M., Condon, L. E., Kollet, S. J., Maher, K., Haggerty, R., & Forrester, M. M. (2016). The imprint of climate and geology on the residence times of groundwater. *Geophysical Research Letters*, *43*(2), 701–708. https://doi.org/10.1002/2015GL066916

McDonnell, J. J., McGuire, K., Aggarwal, P., Beven, K. J., Biondi, D., Destouni, G., Dunn, S., James, A., Kirchner, J., Kraft, P., Lyon, S.,

Maloszewski, P., Newman, B., Pfister, L., Rinaldo, A., Rodhe, A., Sayama, T., Seibert, J., Solomon, K., … Wrede, S. (2010). How old is streamwater? Open questions in catchment transit time conceptualization, modelling and analysis. *Hydrological Processes*, *24*(12), 1745–1754. https://doi.org/10.1002/hyp.7796

McGuire, K. J., & McDonnell, J. J. (2006). A review and evaluation of catchment transit time modeling. *Journal of Hydrology*, *330*(3–4), 543–563. https://doi.org/10.1016/j.jhydrol.2006.04.020

McGuire, K. J., McDonnell, J. J., Weiler, M., Kendall, C., McGlynn, B. L., Welker, J. M., & Seibert, J. (2005). The role of topography on catchment-scale water residence time: Catchment-scale water residence time. *Water Resources Research*, *41*(5), 5002. https://doi.org/10.1029/2004WR003657

Mosquera, G. M., Segura, C., Vaché, K. B., Windhorst, D., Breuer, L., & Crespo, P. (2016). *Insights on the water mean transit time in a high-elevation tropical ecosystem* (preprint). Catchment hydrology/Modelling approaches. https://doi.org/10.5194/hess-2015-546

National Ecological Observatory Network (NEON). (2023a). *Data portal*. https://www.neonscience.org/data

National Ecological Observatory Network (NEON). (2023b). *About NEON*. https://www.neonscience.org/about

National Ecological Observatory Network (NEON). (2023c). *Stable isotopes in precipitation (DP1.00038.001)*. https://data.neonscience.org

National Ecological Observatory Network (NEON). (2023d). *Stable isotopes in surface water (DP1.20206.001)*. https://data.neonscience.org

National Ecological Observatory Network (NEON). (2023e). *Spatial data & maps*. https://www.neonscience.org/data-samples/data/spatial-data-maps

Rhea, S., Gubbins, N., DelVecchia, A. G., Ross, M. R. V., & Bernhardt, E. S. (2023). User-focused evaluation of National Ecological Observatory Network streamflow estimates. *Scientific Data*, *10*(1), 89. https://doi.org/10.1038/s41597-023-01983-w

Rodell, M., Houser, P. R., Jambor, U., Gottschalck, J., Mitchell, K., Meng, C.-J., Arsenault, K., Cosgrove, B., Radakovich, J., Bosilovich, M., Entin, J. K., Walker, J. P., Lohmann, D., & Toll, D. (2004). The global land data assimilation system (GLDAS). *Bulletin of the American Meteorological Society*, *85*(3), 381–394.

SanClements, M., Lee, R. H., Ayres, E. D., Goodman, K., Jones, M., Durden, D., Thibault, K., Zulueta, R., Roberti, J., Lunch, C., & Gallo, A. (2020). Collaborating with NEON. *Bioscience*, *70*(2), 107. https://doi.org/10.1093/biosci/biaa005

Schumer, R., Benson, D. A., Meerschaert, M. M., & Baeumer, B. (2003). Fractal mobile/immobile solute transport: Fractal mobile-immobile solute transport. *Water Resources Research*, *39*(10), 1296. https://doi.org/10.1029/2003WR002141

Segura, C. (2021). Snow drought reduces water transit times in headwater streams. *Hydrological Processes*, *35*(12), e14437. https://doi.org/10.1002/hyp.14437

Stockinger, M. P., Bogena, H. R., Lücke, A., Diekkrüger, B., Cornelissen, T., & Vereecken, H. (2016). Tracer sampling frequency influences estimates of young water fraction and streamwater transit time distribution. *Journal of Hydrology*, *541*, 952–964. https://doi.org/10.1016/j.jhydrol.2016.08.007

Thornton, M. M., Shrestha, R., Wei, Y., Thornton, P. E., Kao, S.-C., & Wilson, B. E. (2022). *Daymet: Daily surface weather data on a 1-km grid for North America, version 4 R1*. ORNL DAAC. https://doi.org/10.3334/ORNLDAAC/2129

U.S. Geological Survey (USGSa), The National Map (TNM), Version 2.0. (2023). *1/3 arc-second Digital Elevation Model (DEM)*. https://apps.nationalmap.gov/downloader/

van Meerveld, H. J. I., Kirchner, J. W., Vis, M. J. P., Assendelft, R. S., & Seibert, J. (2019). Expansion and contraction of the flowing stream network alter hillslope flowpath lengths and the shape of the travel time distribution. *Hydrology and Earth System Sciences*, *23*(11), 4825–4834. https://doi.org/10.5194/hess-23-4825-2019

Virtanen, P., Gommers, R., Oliphant, T. E., Haberland, M., Reddy, T., Cournapeau, D., Burovski, E., Peterson, P., Weckesser, W., Bright, J., van der Walt, S. J., Brett, M., Wilson, J., Millman, K. J., Mayorov, N., Nelson, A. R. J., Jones, E., Kern, R., Larson, E., … Vázquez-Baeza, Y. (2020). SciPy 1.0: Fundamental algorithms for scientific computing in python. *Nature Methods*, *17*(3), 261–272. https://doi.org/10.1038/s41592-019-0686-2

von Freyberg, J., Allen, S. T., Seeger, S., Weiler, M., & Kirchner, J. W. (2018). Sensitivity of young water fractions to hydro-climatic forcing and landscape properties across 22 Swiss catchments. *Hydrology and Earth System Sciences*, *22*(7), 3841–3861. https://doi.org/10.5194/hess-22-3841-2018

Wagener, T., Sivapalan, M., Troch, P. A., McGlynn, B. L., Harman, C. J., Gupta, H. V., Kumar, P., Rao, P. S. C., Basu, N. B., & Wilson, J. S. (2010). The future of hydrology: An evolving science for a changing world: Opinion. *Water Resources Research*, *46*(5), W05301. https://doi.org/10.1029/2009WR008906

Wassenaar, L. I., Terzer-Wassmuth, S., Douence, C., Araguas-Araguas, L., Aggarwal, P. K., & Coplen, T. B. (2018). Seeking excellence: An evaluation of 235 international laboratories conducting water isotope analyses by isotope-ratio and laser-absorption spectrometry. *Rapid Communications in Mass Spectrometry*, *32*(5), 393–406. https://doi.org/10.1002/rcm.8052

Waterisotopes.org for Isoscapes. (2023). https://wateriso.utah.edu/waterisotopes/index.html

Yoshimura, K., Kanamitsu, M., Noone, D., & Oki, T. (2008). Historical isotope simulation using reanalysis atmospheric data. *Journal of Geophysical Research*, *113*(D19), D19108. https://doi.org/10.1029/2008JD010074

How to cite this article: Butler, Z., Good, S., Haagsma, M., Segura, C., & Hu, H. (2023). Relationship between isotope ratios in precipitation and stream water across watersheds of the National Ecological Observation Network. *Hydrological Processes*, *37*(11), e15018. https://doi.org/10.1002/hyp.15018